HAL AEROTHON 2025

Team Isentropic

RV College of Engineering

Department of Aerospace Engineering

TEAM MEMBERS

Prajwal N	prajwaln.ae22@rvce.edu.in
Tushar Mongia	tusharmongia.ae22@rvce.edu.in
Garimella Vihaan Snuhith	gvihaans.ae23@rvce.edu.in
Rahul O M	rahulom.ae23@rvce.edu.in

GITHUB:
https://github.com/RahulOragu/DIHITAL-TWIN-OF-FUEL-SYSTEM-OF-ARDIDEN1H1

Contents

List of Tables

List of Figures

SECTION 1
INTRODUCTION

1 Introduction

The advancement of Digital Twin technology has opened new frontiers in aircraft system monitoring and predictive maintenance. **This project develops a high-fidelity Digital Twin of the fuel injection system for the Turbomeca Shakti 1H1 engine powering HAL's Dhruv Advanced Light Helicopter, with specific focus on:**

- Real-time replication of the Shakti engine's **fuel flow dynamics** and **injection parameters**
- Simulation of critical failure modes including:
  - Fuel probe sensor failures with model-based quantity estimation
  - Injector clogging under particulate contamination
  - Pressure regulator faults affecting power turbine speed
- Health monitoring of:
  - Injector spray pattern degradation
  - Fuel coking risks during prolonged idle
  - Vibration-correlated anomalies

The implementation integrates **Shakti engine-specific parameters** from operational manuals with **Dhruv HUMS data** to create a physics-accurate virtual model. The Digital Twin serves three critical functions for rotary-wing operations:

1. **Maintenance Optimization**: Reducing AOG (Aircraft on Ground) time through early fault detection
2. **Flight Safety Enhancement**: Predicting fuel starvation risks during autorotation
3. **Legacy System Integration**: Complementing Dhruv's existing Health Usage Monitoring System (HUMS)

Figure 1: Shakti 1H1 engine fuel system schematic (adapt as needed)

CHAPTER 2

SELECTION OF FUEL INJECTION SYSTEM

2 Selection of Fuel Injection System

The digital twin development requires careful selection of an appropriate fuel injection system architecture. We evaluate two predominant systems for helicopter applications: the Common Rail System (CRS) and Multi-Pump System (MPS).

2.1 System Architectures

0.3

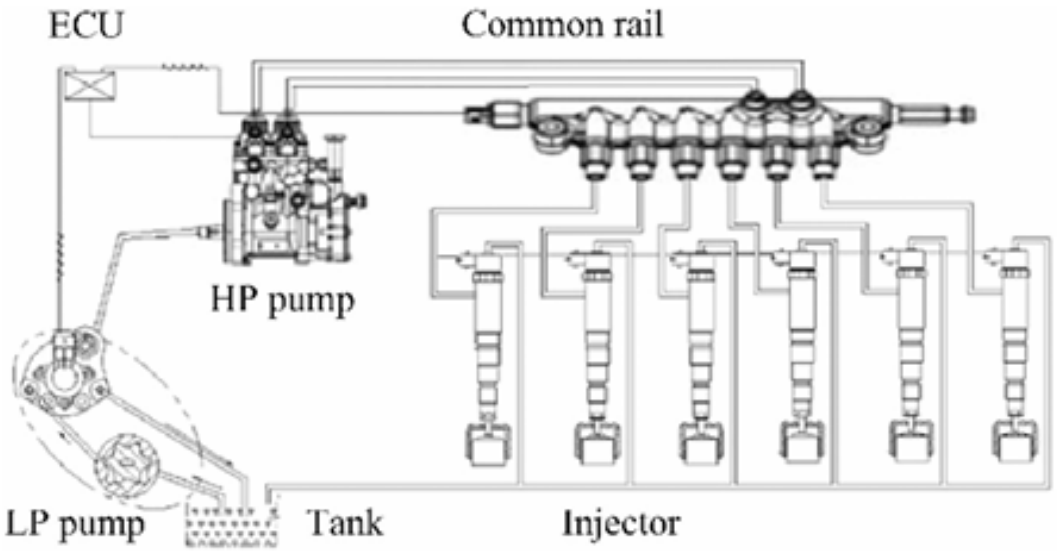

Figure 2: Common Rail System (CRS)

0.3

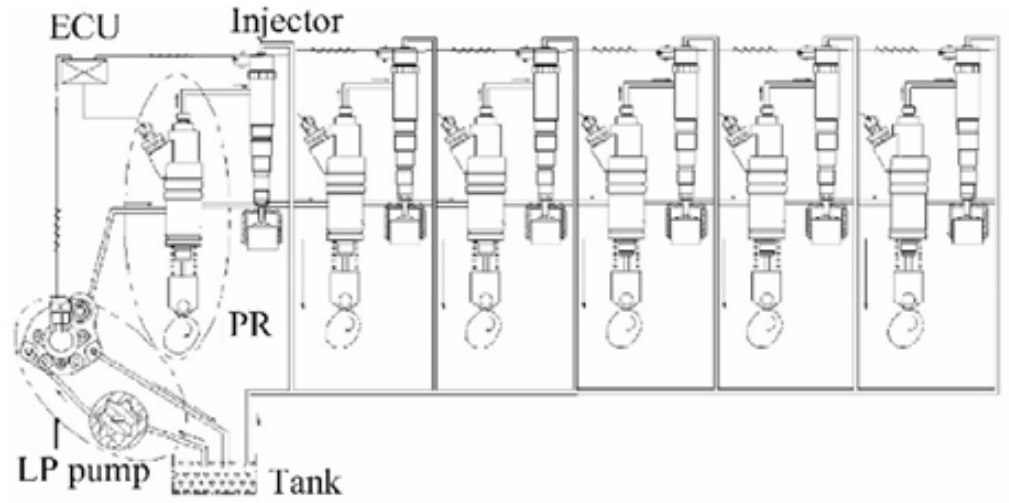

Figure 3: Multi-Pump System (MPS)

Figure 4: Comparative schematics of fuel injection system architectures. CRS (left) features centralized high-pressure rail, while MPS (right) employs distributed pumping units.

2.2 Comparative Performance Analysis

Table 1: Quantitative Comparison of Injection System Performance Characteristics

Parameter	CRS	MPS	Unit
Pressure Fluctuation	100%	43%	(Baseline)
Pre-injection Stability	Unstable	Stable	–
Rail/Reservoir Volume	18.84	10.00	cm^3
Response Time	50	30	ms
Cylinder Interference	High	None	–
Maintenance Complexity	High	Moderate	–

2.3 Technical Evaluation

2.3.1 Common Rail System Limitations

- **Pressure Dynamics:**
  - Exhibits 6 pressure waves/cycle at 1900 rpm [**?**]
  - ΔP = 2-3 MPa during injection events
  - Results in ±5% fuel quantity variation between cylinders
- **Transient Response:**
  - Minimum 4 ms damping time between injections
  - Limited ECU compensation capability for rapid pressure changes

2.3.2 Multi-Pump System Advantages

- **Pressure Control:**
  - 57% lower pressure fluctuation (p less than 0.01) [**?**]
  - 40 ms pressure recovery window
  - Independent per-cylinder pressure regulation
- **Design Features:**
  - 47% smaller reservoir volume requirement
  - Eliminates high-pressure interconnecting piping
  - Modular maintenance capability

2.4 Selection Rationale

The MPS architecture is selected for digital twin development based on:

1. Superior pressure stability (critical for failure mode simulation)
2. Demonstrated performance in experimental validation:

$$\frac{\sigma_{CRS}}{\sigma_{MPS}} = 2.33 \quad (\text{p ¡ } 0.05) \tag{1}$$

3. Built-in hardware redundancy
4. Enhanced condition monitoring capability through:
   - Per-cylinder pressure sensors
   - Isolated failure domains
   - Individual pump health metrics

CHAPTER 3
SYSTEM REQUIREMENTS

3 MPS Injector System Requirements

3.1 Tier 1 Requirements Table — MPS Injector System

ID	Tier 1 Requirement (High-Level System Need)
T1-R1	The MPS injector system shall ensure continuous and correct fuel delivery under all operating conditions
T1-R2	The injector assembly shall provide reliable injection performance without mechanical or electrical failure
T1-R3	The control system shall command accurate fuel flow matching engine demand

3.2 Tier 2 Requirements Table

ID	Parent	Tier 2 Requirement (Detailed Need)
T2-R1	T1-R1	The system shall detect and report fuel starvation conditions (e.g. low pressure, airlock)
T2-R2	T1-R1	The system shall include redundant fuel supply path or blockage warning system
T2-R3	T1-R1	The system shall detect fuel tank vent failure and alert the crew
T2-R4	T1-R2	The injector shall have health monitoring for solenoid operation
T2-R5	T1-R2	The injector mechanical components shall meet vibration endurance standards
T2-R6	T1-R2	Connectors shall be secured against loosening under vibration
T2-R7	T1-R2	The injector shall be protected against fatigue-induced damage of housing/harness
T2-R8	T1-R3	Feedback sensors shall have redundancy for critical parameters (pressure, temperature)
T2-R9	T1-R3	The software logic shall include fail-safes for corrupted commands (e.g. watchdogs, cross-checks)
T2-R10	T1-R3	The system shall withstand transient power events without erroneous fuel command

CHAPTER 4

SYSTEM SAFETY ASSESSMENT (SSA)

4 FMEA – Failure Mode and Effects Analysis

Table 2: **FMEA – Failure Mode and Effects Analysis**

Failure Mode	Potential Effect(s)	S	O	D	RPN	Recommended Action
Fuel line blockage	Engine flameout	10	4	5	200	Install blockage detection sensor; enhance fuel filtration
Fuel line blockage	Partial power loss → mission degradation	8	4	5	160	
Fuel pump degraded / failed	Insufficient fuel → power fluctuation	8	3	6	144	Health monitoring; preventive replacement schedule
Fuel pump degraded / failed	Failure to start engine	9	2	7	126	Pre-start pump checks
Airlock / vapor lock	Engine flameout	10	2	8	160	Air purge system; venting improvements
Airlock / vapor lock	Power oscillation / misfire	7	2	8	112	
Injector nozzle clogged	Uneven fuel delivery → vibration, power loss	8	4	5	160	Self-cleaning nozzle; periodic flushing
Injector nozzle clogged	Increased emissions / efficiency loss	6	4	5	120	
Injector solenoid failure	No injection → power loss	9	3	6	162	Solenoid health monitoring; redundancy
Injector solenoid failure	Misfire → vibration, damage risk	7	3	6	126	
Electrical connector failure (injector)	Complete loss of injection → engine power loss	10	5	6	300	Improved connectors; vibration-proof design; inspection
Electrical connector failure (injector)	Intermittent injection → engine instability	8	5	6	240	
Feedback sensor failure (pressure, temp)	Wrong fuel command → power loss	8	4	7	224	Redundant sensors; cross-checking logic
Feedback sensor failure	Rich mixture → excessive fuel burn, thermal risk	7	4	7	196	
Feedback sensor failure	Incorrect injection timing → engine damage risk	9	2	9	180	
Software / FADEC error	Poor fuel economy → mission range impact	7	2	9	126	Rigorous validation; independent logic; Digital Twin cross-check
Software / FADEC error						
Vibration-induced fatigue (harness, mount)	Connector failure → loss of injection	9	4	7	252	Strengthen mounts; isolate harnesses; better clamps
Vibration-induced fatigue (harness, mount)	Intermittent signals → unstable engine output	8	4	7	224	
Fuel probe sensor failure	Undetected fuel starvation → flameout	10	3	7	210	Dual redundant probes; flow cross-check
Fuel probe sensor failure	False low fuel warning → unnecessary landing	6	3	7	126	

4.1 Inference from FMEA Analysis

The red-highlighted rows in the FMEA table correspond to failure modes with **red**Risk Priority Numbers (RPN) ≥ 200, indicating highly critical failure conditions in the MPS injector system. These include:

- Electrical connector failures leading to complete loss of injection or engine instability.
- Feedback sensor errors causing incorrect fuel commands.
- Vibration-induced fatigue compromising connectors or engine output.

- Fuel probe sensor faults resulting in undetected fuel starvation and flameout.

Such failures have the potential to cause **engine flameout, power loss, or unstable combustion**, making them safety-critical. Therefore, these high-RPN issues should be prioritized with **redundancy, health monitoring, robust design, and validation strategies** to ensure reliable and safe operation of the injector system.

4.2 FTA – Fault Tree Analysis

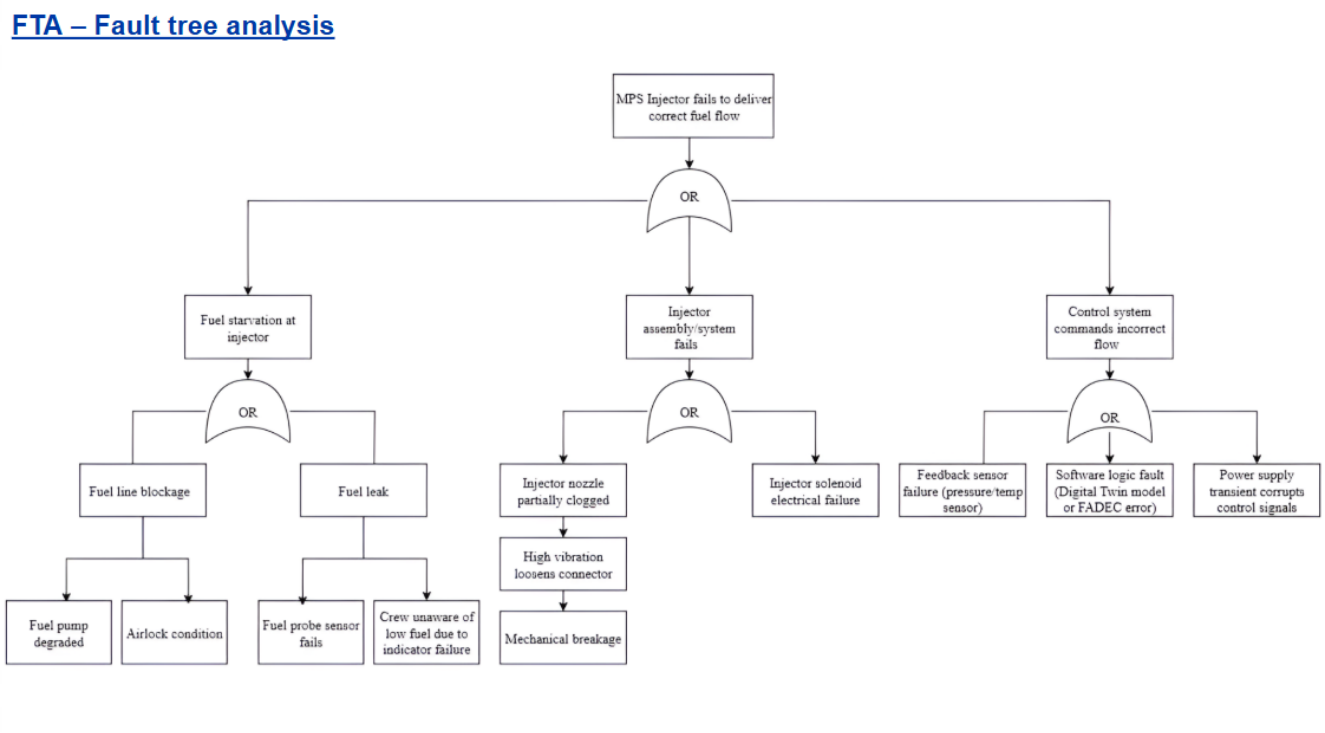

Figure 5: Fault Tree Analysis for MPS Injector System

Inference:

The Fault Tree Analysis (FTA) reveals that failure of the MPS injector system to deliver correct fuel flow can result from multiple causes. These are categorized under three primary branches: fuel starvation at the injector, injector assembly/system failures, and control system command errors. **Contributing factors include fuel line blockage, vibration-induced connector faults, sensor and solenoid failures, and software or power anomalies. The structure highlights the critical role of redundancy, sensor accuracy, and mechanical robustness in avoiding catastrophic injection failure.Mitigation should focus on breaking fault propagation paths and improving detection mechanisms.**

CHAPTER 5

DETAILED DESIGN REVIEW AND CALCULATIONS

5 Detailed Design Review

5.1 Plunger Control Mechanism and Spool Orifice Dynamics

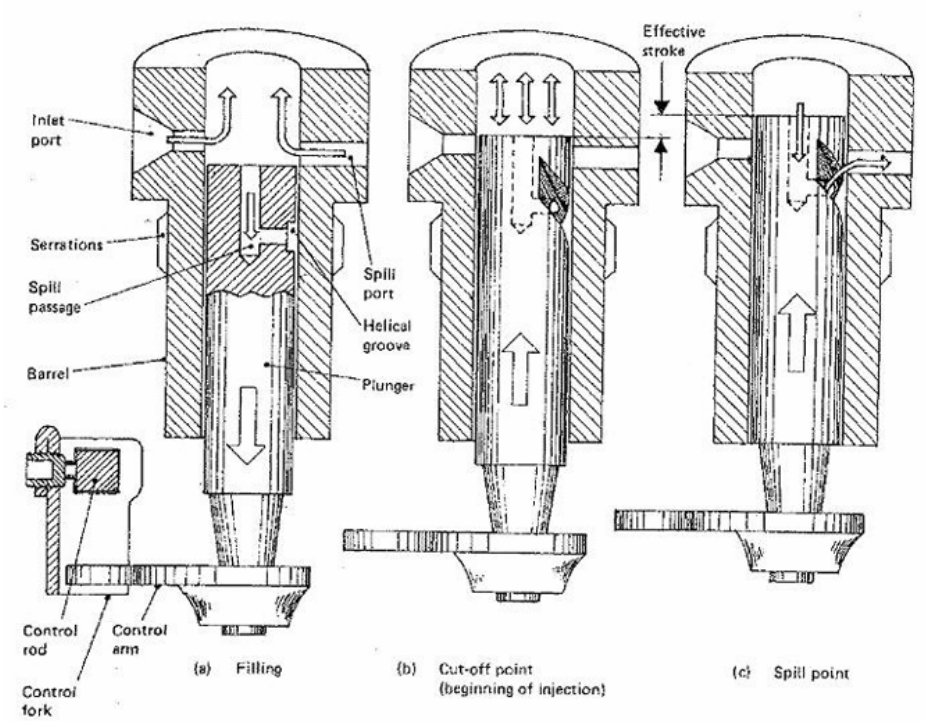

Figure 2: Plunger Interaction with Control Orifices in the Barrel

Figure 6: Plunger Interaction with Control Orifices in the Barrel
Adapted for comparison with Engine In-Line Injection System – Simulink Reference Model [2]
`https://www.mathworks.com/help/autoblks/ug/diesel-engine-in-line-injection-system.html`

The plunger control mechanism in the MPS injector system regulates the timing and quantity of fuel injection using three control orifices:

- **Inlet Port**
- **Spill Port**
- **Helical Groove–Spill Port Orifice**

These orifices are modeled as variable-area Spool Orifice (IL) blocks and function based on the following assumptions:

1. The opening of the inlet and spill ports is directly dependent on the linear displacement of the plunger.
2. The helical groove forms a variable orifice with the spill port, whose opening depends on both the linear motion and the rotational displacement of the plunger.

3. For simplification in the control model, plunger rotation is represented as an effective linear displacement superimposed on the plunger motion.

The figure above illustrates three key phases of the plunger's operation:

- **Filling Phase (a):** The inlet port is open, allowing fuel to fill the barrel chamber.
- **Cut-off Point (b):** The start of injection occurs as the plunger moves upward and seals the inlet port.
- **Spill Point (c):** The helical groove aligns with the spill port, ending the injection phase as excess fuel escapes.

This interaction precisely controls fuel quantity and timing for each injection event, and the dimensional parameters derived from this model are critical for the simulation of the control orifice dynamics in MATLAB or AMESim.

5.2 Injection Plunger Dimensional Parameterization

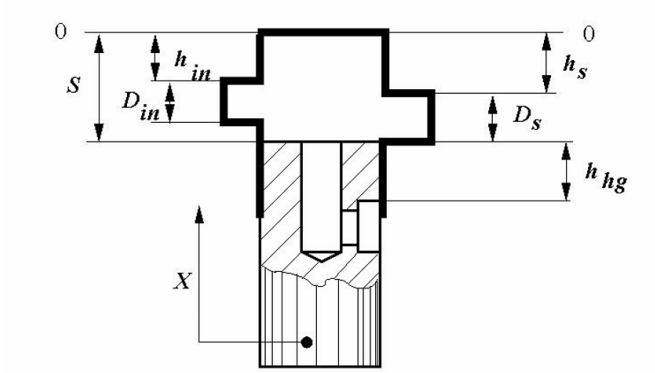

Figure 7: Schematic of injection plunger dimensions
Adapted for comparison with Engine In-Line Injection System – Simulink Reference Model [2]
`https://www.mathworks.com/help/autoblks/ug/diesel-engine-in-line-injection-system.html`

The schematic above defines the key geometric parameters for the injection plunger system. The corresponding variable definitions are as follows:

- D_{in}: Inlet port orifice diameter (`inlet_orifice_diameter`)
- D_s: Spill port orifice diameter (`spill_orifice_diameter`)
- S: Plunger stroke (`plunger_stroke`)
- h_{is}: Distance between the inlet orifice and the top plunger position:

  $h_{is} = -\texttt{plunger\_stroke} + \texttt{safety\_gap} + \texttt{inlet\_orifice\_diameter} + \texttt{inlet\_offset}$
- h_s: Distance between the spill port orifice and the top plunger position:

  $$h_s = -\texttt{plunger\_stroke} + \texttt{safety\_gap} + \texttt{spill\_orifice\_diameter}$$
- h_{hg}: Distance between the spill port orifice and the upper edge of the helical groove

The inlet orifice is generally located higher than the spill orifice. This difference in height is represented by the parameter `inlet_offset`.

Parameterization Notes:

1. The top of the plunger stroke is set as the origin, and motion upward is considered positive. Hence, the inlet and spill ports must be configured to open with negative spool displacement.

2. The helical groove opens with upward motion and positive spool displacement.

Effective Stroke Control: The plunger's effective stroke is defined as:

$$\texttt{plunger\_stroke} - \texttt{safety\_gap} - \texttt{inlet\_orifice\_diameter} - \texttt{inlet\_offset}$$

The distance h_{hg} (spill port to helical groove) is tunable by rotating the plunger. This controls the point where the spill is triggered by the helical groove opening. As this value decreases, injection duration shortens, since the groove opens sooner. The maximum control signal corresponds to the full effective stroke.

5.3 CAD Model Design

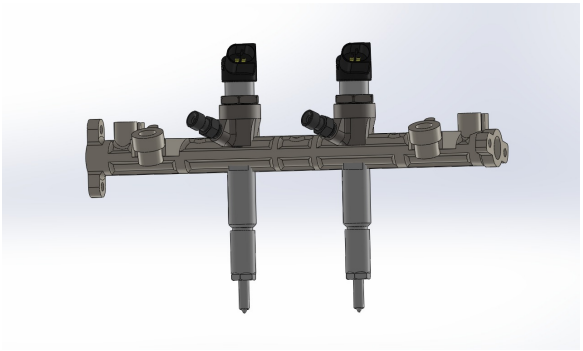

Figure 8: CAD Model – Fuel Injector Assembly

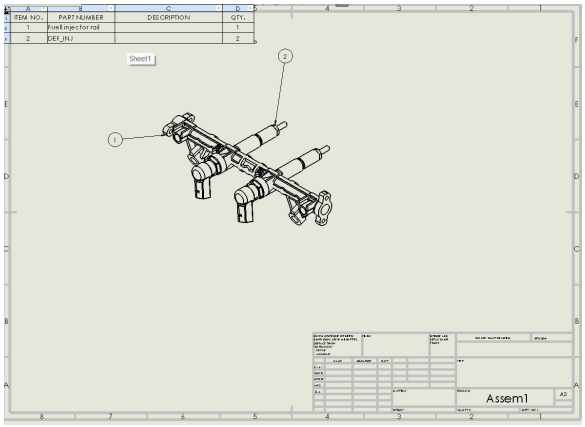

Figure 9: CAD Model – Fuel Pump Unit

5.4 Design Parameters for MPS Injector System

The following parameters are used in the mathematical model of the Multi-Pump System (MPS) for the helicopter's fuel injection:

Table 3: Design Parameters for Injector Calculations

Parameter	Symbol	Value
Plunger Area	A_p	1.14×10^{-4} m^2
Plunger Stroke	h	0.01 m
Dead Volume	V_0	2.6×10^{-6} m^3
Bulk Modulus of Fuel	K	1×10^9 Pa
Viscosity of Fuel	μ	1.5×10^{-3} Pa·s
Density of Fuel	ρ	800 kg/m^3
Injection Time	Δt	0.005 s
Valve Orifice Area	A	2.1×10^{-6} m^2

5.5 Single Injector System Calculations

1. **Maximum Displaced Volume:**
   $V_{max} = A_p \cdot h = 1.14 \times 10^{-4} \times 0.01 = 1.14 \times 10^{-6}$ m^3

2. **Volumetric Flow Rate:**
   $\dot{V} = \frac{V_{max}}{\Delta t} = \frac{1.14 \times 10^{-6}}{0.005} = 2.28 \times 10^{-4}$ m^3/s

3. **Flow Rate Conversion:**
   $\dot{V}_{L/hr} = 2.28 \times 10^{-4} \times 3600 = 820.8$ L/hr

4. **Pressure Rise:**
   $\Delta p = K \cdot \frac{V_{max}}{V_0} = 1 \times 10^9 \cdot \frac{1.14 \times 10^{-6}}{2.6 \times 10^{-6}} = 304.81$ MPa

5. **Orifice Diameter:**
   $d = \sqrt{\frac{4A}{\pi}} = \sqrt{\frac{4 \times 2.1 \times 10^{-6}}{\pi}} = 1.63$ mm

6. **Fuel Velocity:**
   $v = \frac{\dot{V}}{A} = \frac{2.28 \times 10^{-4}}{2.1 \times 10^{-6}} = 108.57$ m/s

7. **Reynolds Number:**
   $Re = \frac{\rho v d}{\mu} = \frac{800 \cdot 108.57 \cdot 0.00163}{1.5 \times 10^{-3}} = 94,685$

5.6 Summary Table: Single Injector

Table 4: Performance Metrics – Single Injector System

Quantity	Value
Displaced Volume (V_{max})	1.14×10^{-6} m^3
Flow Rate	2.28×10^{-4} m^3/s (820.8 L/hr)
Pressure Rise	304.81 MPa
Velocity	108.57 m/s
Reynolds Number	94,685

5.7 Four Injector System Calculations

1. **Total Flow Rate:**
   $\dot{V}_{total} = 4 \times 820.8 = 3,283.2$ L/hr or 9.12×10^{-4} m^3/s
2. **Total Displaced Volume:**
   $V_{total} = 4 \times 1.14 \times 10^{-6} = 4.56 \times 10^{-6}$ m^3
3. **Reynolds Number (per injector):**
   $Re = 94,685$ (same as single injector)

5.8 Summary Table: Four Injector System

Table 5: Performance Metrics – Four Injector System

Quantity	Value
Total Flow Rate	3,283.2 L/hr
Total Displaced Volume	4.56×10^{-6} m^3
Per Injector Flow Rate	820.8 L/hr
Flow Rate (SI Units)	9.12×10^{-4} m^3/s
Reynolds Number (per injector)	94,685

5.9 Final Design Outcome

The detailed calculations confirm that the designed MPS injector system achieves the following:

- **High injection pressure:** 304.81 MPa
- **High volumetric flow rate:** 820.8 L/hr per injector

- **Turbulent flow regime:** $Re = 94,685$
- **Fast injection response time:** 5 ms duration per cycle

These outcomes validate the MPS architecture's capability for high-performance, precision-controlled fuel injection suitable for turboshaft helicopter engines.

5.10 Fuel Property Calculations

The following empirical correlations from Zhang et al. (2018) were used to estimate fuel properties (diesel) under operating conditions of 80°C temperature and 160 MPa injection pressure.

5.11 Input Conditions

Parameter	**Value**
Temperature, T	80°C
Pressure, p	160 MPa

Table 6: Operating Conditions for Fuel Property Estimation

5.12 1. Fuel Density Calculation

Empirical correlation:

$$\rho = (199 - 0.1T) \cdot \exp\left[0.54\,(p + 111061456.8 - 469742.3T)^{0.053}\right]$$

Substituting values:

$$\rho = (199 - 0.1 \times 80) \cdot \exp\left[0.54\left(160 \times 10^6 + 111061456.8 - 469742.3 \times 80\right)^{0.053}\right]$$

$$\rho = 191 \cdot \exp\left[0.54 \cdot (233582096.8)^{0.053}\right] = 191 \cdot \exp(0.5262) = \boxed{855.47\,\mathrm{kg/m^3}}$$

5.13 2. Fuel Viscosity Calculation

Empirical correlation:

$$\mu = \exp\left(-6.5496 - \frac{23.5417}{T}\right) + 1.38 \times 10^{-8} \cdot \exp\left(\frac{2.9014}{T}\right) \cdot T^{-1.5059}$$

Substituting values:

$$\mu = \exp\left(-6.5496 - \frac{23.5417}{80}\right) + 1.38 \times 10^{-8} \cdot \exp\left(\frac{2.9014}{80}\right) \cdot 80^{-1.5059}$$

$$= \exp(-6.843) + 1.38 \times 10^{-8} \cdot \exp(0.0363) \cdot 0.007 = \boxed{1.066 \times 10^{-3}\,\mathrm{Pa{\cdot}s}}$$

3. Fuel Bulk Modulus Calculation

Empirical correlation:

$$K = 34.74 \cdot (p + 111061456.8 - 469742 \cdot T)^{0.947}$$

Substituting values:

$$K = 34.74 \cdot \left(160 \times 10^6 + 111061456.8 - 469742 \cdot 80\right)^{0.947}$$

$$= 34.74 \cdot (233582096.8)^{0.947} = \boxed{2.921 \times 10^9\,\text{Pa} = 2.921\,\text{GPa}}$$

5.14 Summary Table: Fuel Properties at 80°C and 160 MPa

Property	**Value**	**Units**
Fuel Density (ρ)	855.47	kg/m^3
Fuel Viscosity (μ)	1.066×10^{-3}	Pa·s
Fuel Bulk Modulus (K)	2.921×10^9	Pa (2.921 GPa)

Table 7: Estimated Fuel Properties

CHAPTER 6

ARCHITECTURE AND FADEC IMPLEMENTATION

6 Architecture and FADEC Implementation

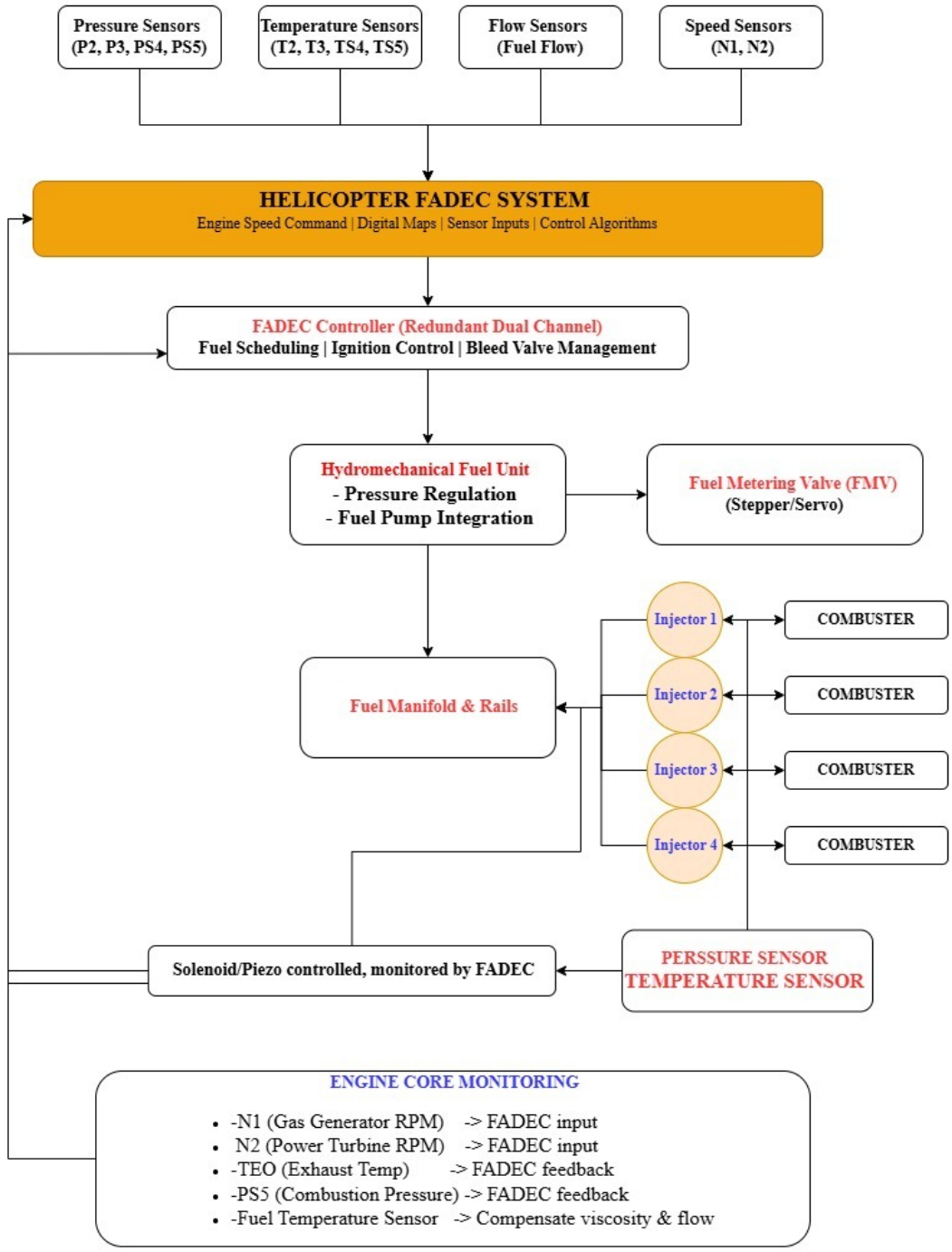

Figure 10: Block Diagram of Dual Channel FADEC-Based Fuel Injection System

6.1 System Overview

The Full Authority Digital Engine Control (FADEC) system is a critical component for managing helicopter turboshaft engine performance. The above architecture represents a dual-channel FADEC configuration, which provides redundancy and ensures safe and optimal engine operation during all flight regimes.

6.2 FADEC Inputs and Sensor Integration

The FADEC receives continuous real-time data from multiple sensor types:

- **Pressure Sensors** (e.g., P2, P3, PS4, PS5) — Monitor air and combustion pressures.
- **Temperature Sensors** (e.g., T2, T3, T4, T5) — Track air and fuel temperature at various stages.
- **Flow Sensors** — Measure fuel flow rate.
- **Speed Sensors** (N1, N2) — Monitor engine shaft speeds:
  - N1: Gas generator RPM
  - N2: Power turbine RPM

6.3 Dual Channel FADEC Controller

The controller unit performs key functions:

- Fuel scheduling and metering
- Ignition control
- Bleed valve management
- Health monitoring

Each channel of the FADEC works independently and continuously cross-checks with the redundant channel to ensure fail-safe operation.

6.4 Hydromechanical Unit and Fuel Metering

The hydromechanical unit integrates a high-pressure fuel pump with a pressure regulator. It supplies fuel to a **Fuel Metering Valve (FMV)** which is operated via a stepper or servo motor and is directly modulated by the FADEC output signal. The FMV precisely controls the quantity of fuel supplied to the injectors.

6.5 Injector and Rail Distribution System

Fuel from the metering system is distributed through a common **Fuel Manifold and Rail System** to the four individual injectors. Each injector supplies fuel to a dedicated combustor chamber.

6.6 Monitoring and Feedback Loop

Key sensors provide closed-loop feedback for real-time correction:

- **Exhaust Temperature (TBO)** — Used for thermal feedback
- **Combustion Pressure (PS5)** — Used for pressure-based fuel modulation
- **Fuel Temperature Sensor** — Compensates for viscosity and flow variations

6.7 Engine Core Monitoring Summary

- N1 (Gas Generator RPM) → FADEC input
- N2 (Power Turbine RPM) → FADEC input
- TBO (Exhaust Temp) → FADEC feedback
- PS5 (Combustion Pressure) → FADEC feedback
- Fuel Temperature Sensor → Flow compensation

This architecture allows for seamless integration of real-time sensor data, advanced control algorithms, and health monitoring — enabling optimal fuel efficiency, minimal emissions, and robust safety.

CHAPTER 7

DIGITAL TWIN OF HELICOPTER FUEL INJECTION SYSTEM

7 Digital Twin of Helicopter Fuel Injection System

7.1 System Overview

The Digital Twin provides real-time simulation of the Ardiden 1 helicopter fuel system with the following capabilities:

- **Real-time Monitoring**: Live visualization of fuel system parameters
- **Fault Simulation**: Injection of 10+ failure scenarios
- **Interactive Controls**: Throttle adjustment and system manipulation

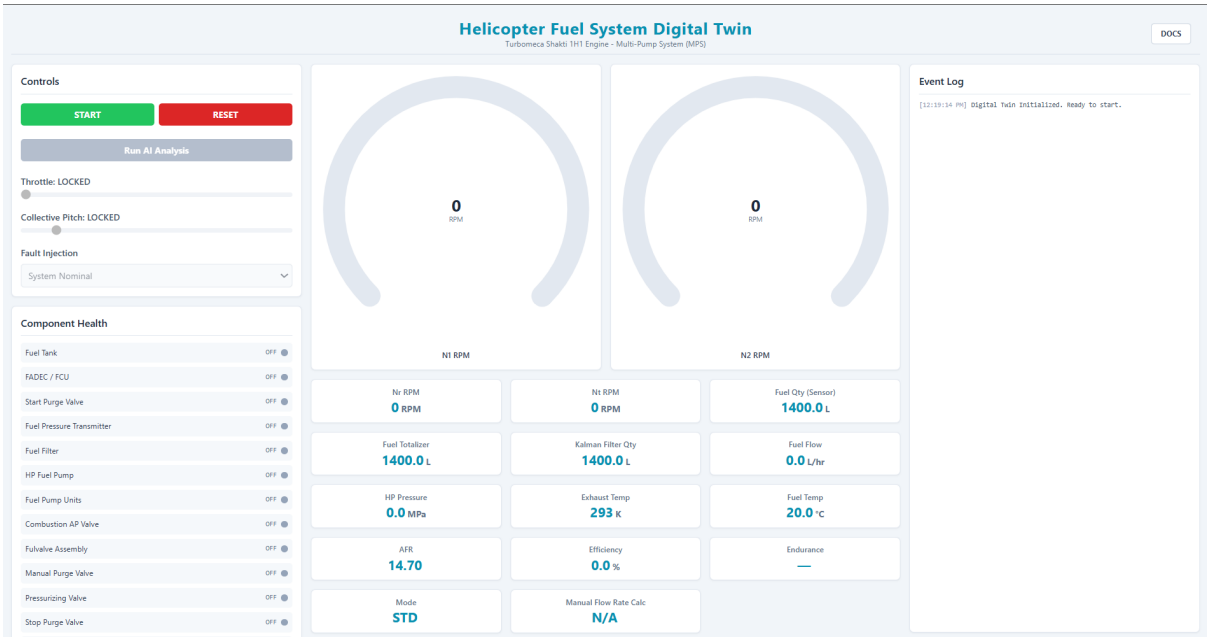

Figure 11: Digital Twin Dashboard showing , Throttle controls, RPM gauges,Health indicators, and Event log

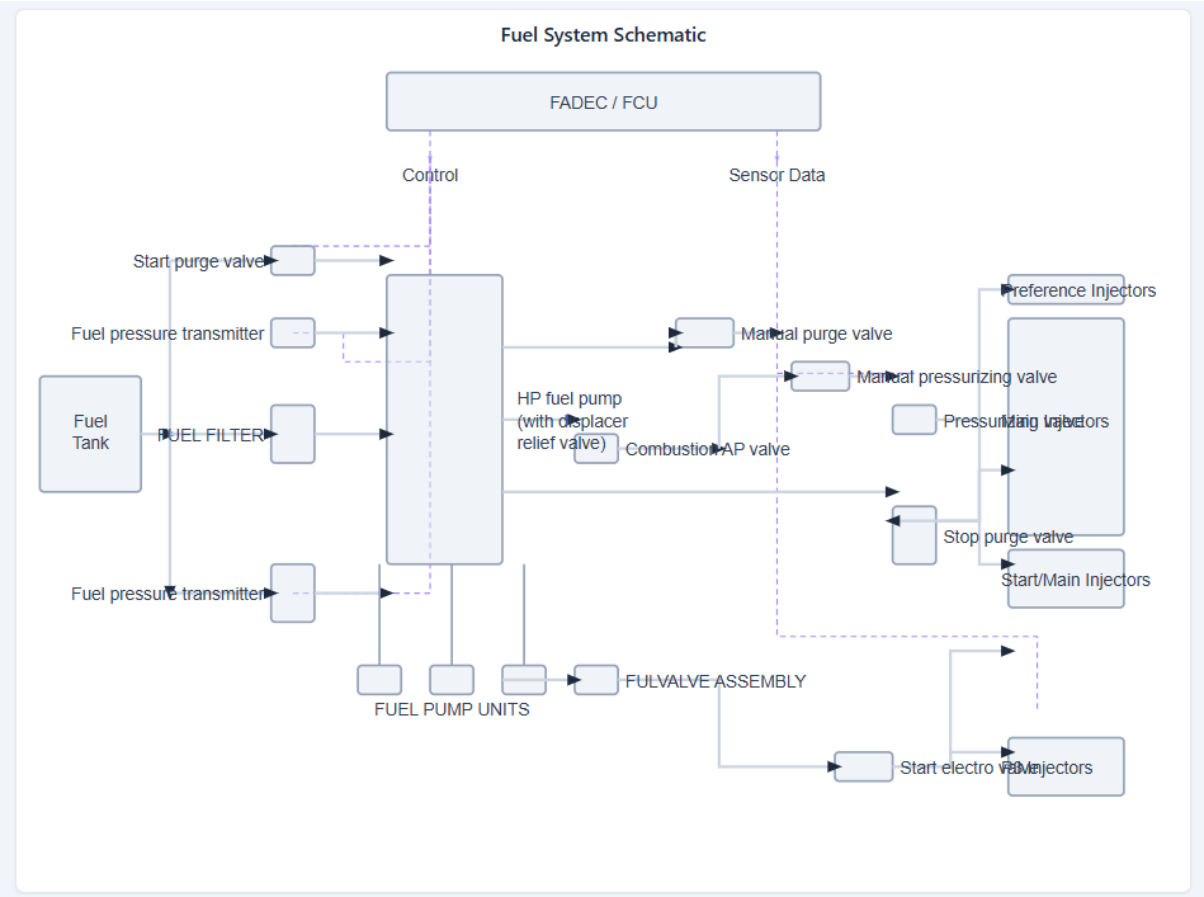

Figure 12: Digital Twin Dashboard showing Fuel system schematic

7.2 Technical Specifications

7.2.1 System Components

Table 8: System Components of the Digital Twin Interface

Component	Description
Control Panel	Contains throttle slider (0–100%) and fault injection interface
RPM Gauges	Dual displays for N1 (0–1400) and N2 (0–293) RPM values
System Schematic	Interactive SVG diagram showing fuel flow and component status
Health Indicators	Color-coded status bars for all major components
Event Log	Timestamped record of system events and warnings

7.2.2 Simulation Parameters

Table 9: Simulation Parameters for Digital Twin Model

Parameter	Range	Unit
Throttle Position	0–100	%
N1 RPM	0–1400	rpm
N2 RPM	0–293	rpm
Fuel Flow Rate	0–50	kg/hr
System Pressure	0–500	kPa

7.2.3 Complete Project Structure

Listing 1: Directory structure of the Digital Twin front-end project

```
|-- index.html # Main HTML entry point
|-- index.tsx # React entry point
|-- metadata.json # Application metadata
|-- App.tsx # Root component with state management
|
|-- components/
| |-- ChartCard.tsx # Time-series chart component
| |-- ControlPanel.tsx # Throttle and fault controls
| |-- Dashboard.tsx # Main layout grid
| |-- DataCard.tsx # Single metric display
| |-- Documentation.tsx # Help system
| |-- Gauge.tsx # Circular RPM gauge
| |-- Header.tsx # Top navigation
| |-- HealthStatusCard.tsx # Component health bars
| |-- LogCard.tsx # Event log display
| |-- SystemSchematic.tsx # Interactive SVG diagram
|
|-- services/
| |-- simulationService.ts # Core simulation logic
|
|-- constants.ts # System parameters
|-- types.ts # TypeScript type definitions
```

7.3 Implementation Details

7.3.1 Technology Stack

```
Frontend: React v19 + TypeScript
Visualization: Recharts + SVG
Styling: TailwindCSS
State Management: React useReducer
Build: ESM Modules via CDN
```

7.3.2 Data Flow Architecture

1. User interactions trigger state updates
2. Simulation service processes physics model
3. Updated state propagates to visual components
    - Gauges receive RPM values
    - Schematic updates component status
    - Event log records system changes
4. Cycle repeats every 500ms (2Hz update rate)

7.4 Fault Injection System

Table 10: Fault Injection Scenarios for the Digital Twin

Fault Type	Target	Effect	Severity
Sensor Bias	RPM Sensors	±15% error in rotational speed reading	1–3
Complete Failure	Fuel Probe	No fuel level signal received	4
Intermittent	Wiring	Random signal dropouts causing instability	2–5
Blockage	Fuel Line	Reduced fuel flow rate and pressure loss	3–8

7.5 Deployment

- **Requirements**: Modern web browser only
- **Launch**:
    - `npx serve` (Node.js)
    - `python -m http.server` (Python 3)
- **Access**: http://localhost:3000

7.6 Helicopter Fuel System Digital Twin

This interactive simulation models the Multi-Pump Fuel Injection System (MPS) of a Turbomeca Shakti 1H1 engine. Its purpose is to provide a high-fidelity environment for:

- Real-time monitoring
- Performance analysis
- Study of failure modes

7.6.1 System Schematic Explained

Visual representation of fuel flow from tank to injectors. Component status indicators:

- Green border: Normal operation
- Yellow border: Warning state
- Red border: Fault condition

Key Components

Fuel Tank Source of fuel. Status changes:

- WARN on low fuel
- FAULT when empty

HP Fuel Pump Increases fuel pressure. Performance tied to N1 RPM.

Fuel Filter Removes contaminants. Blockage reduces downstream pressure/flow.

FADEC/FCU System controller that:

- Monitors all sensors
- Manages fuel flow
- Controls engine RPM
- Ensures optimal/safe operation

Valves Direct fuel flow during:

- Engine start-up
- Normal operation
- Shutdown

Injectors Atomize and inject fuel. Flow rate modeled based on:

- FADEC commands
- System health

7.6.2 Core Simulation Logic

The simulation runs on discrete clock cycles. Each tick recalculates system state based on:

- Previous state
- User inputs
- Governing formulas (detailed below)

7.6.3 Dashboard Data Cards

N1/N2 RPM Gauges

- N1: Gas generator speed
- N2: Power turbine speed
- Calculation:

$$\text{Target N1} = \text{Idle N1} + \left(\frac{\text{Throttle}}{100}\right) \times (\text{Max N1} - \text{Idle N1})$$

Nr/Nt RPM

- Governor correction:

$$\text{Correction} \propto (\text{Target Nr} - \text{Current Nr})$$

Fuel Quantity Sensor

- During faults:

$$\text{Fuel Qty} = \text{True Fuel} + \text{Slosh Noise}$$

Fuel Totalizer

- Ground truth calculation:

$$\text{New Fuel} = \text{Prev Fuel} - \left(\text{Flow} \times \frac{\text{Tick Rate}}{3.6 \times 10^6}\right)$$

Kalman Filter Qty

- Core update logic:

$$\text{New Value} = \text{Prediction} + \text{Gain} \times (\text{Sensor Value} - \text{Prediction})$$

Fuel Flow

- Non-linear model:

$$\text{Flow} \propto (\text{Effective N1 throttle})^{1.2}$$

HP Pressure

- Exponential relationship:

$$\text{Pressure} = \text{Max P} \times \left(\frac{\text{N1 RPM}}{\text{Max N1}}\right)^{1.8}$$

Exhaust Temp (EGT)

- Temperature calculation:

$$\text{EGT} = \text{Idle Temp} + \left(\frac{\text{N1 RPM}}{\text{Max N1}}\right) \times (\text{Max Temp} - \text{Idle Temp})$$

Fuel Temperature

- Heat exchange model:

$$\Delta\text{Temp} \propto (\text{EGT} - \text{Ambient Temp})$$

AFR (Air-Fuel Ratio)

- Dynamic adjustment:

$$\text{AFR} = \text{Base AFR} - (|\Delta\text{Throttle}| \times \text{Factor})$$

Efficiency

- Fault impact model:

$$\text{Efficiency} = \text{Base Efficiency} - \text{Fault Penalties}$$

Endurance

- Flight time estimate:

$$\text{Endurance (hr)} = \frac{\text{Fuel Totalizer}}{\text{Fuel Flow}}$$

7.6.4 FADEC & Fault Injection

FADEC Modes

Standard (STD) Default engine control logic

AFR-Enhanced (AFR+) Provides:

- 8% better fuel efficiency
- 5% more power output
- Faster engine response

Simulated Faults

- **Sensor Bias (N1)**: Incorrect RPM values
- **Blockage Fuel Line**: Pressure drop, EGT increase
- **Fail Fuel Probe**: Fixed incorrect fuel reading

- **Injector Faults**: Power loss and vibration
- **Sloshing Fuel Tank** (selectable intensity):
  - Low: Gentle forward flight
  - Medium: Coordinated banking turn
  - High: Aggressive maneuvers

7.6.5 Kalman Filter Implementation

Two-step process during `SLOSHING_FUEL_TANK` fault:

1. Prediction Step

$$\hat{x}_p = A \cdot x_{\text{prev}}$$
$$P_p = A \cdot P_{\text{prev}} \cdot A^T + Q$$

2. Update Step

$$K = P_p \cdot H^T \cdot (H \cdot P_p \cdot H^T + R)^{-1}$$
$$x = \hat{x}_p + K \cdot (z - H \cdot \hat{x}_p)$$
$$P = (I - K \cdot H) \cdot P_p$$

Measurement Noise (R) is dynamically adjusted based on slosh intensity.

7.6.6 Predictive Maintenance AI Model

Function: "Run AI Analysis" using Gemini LLM as Prognostic Reasoning Module.
Analysis Parameters:

- Mechanical stress cycles (throttle changes)
- Thermal stress events (EGT peaks)
- Efficiency trends
- System state history

Outputs:

- Wear analysis summary
- Component-specific predictions
- Maintenance recommendations

CHAPTER 8

AIR FUEL CONTROL IN FADEC SYSTEM USING FUZZY LOGIC PID CONTROLLER

8 Air fuel control in FADEC system using Fuzzy Logic Controlled PID

This document analyzes the air-fuel ratio (AFR) control implementation from Wang et al.'s paper *"Efficiency optimized fuel supply strategy of aircraft engine based on air-fuel ratio control"* and explains its relationship with Full Authority Digital Engine Control (FADEC) systems.

8.1 Problem Identification

Traditional engine control systems face several limitations:

- Open-loop fuel calibration with fixed fuel maps
- Instability during transient conditions (throttle changes/altitude shifts)
- Results in either:
  - Rich mixtures (wasted fuel)
  - Lean mixtures (power loss risk)
- Limited adaptation to changing flight conditions

8.2 Innovative Solution

The paper proposes a closed-loop AFR control system integrated with FADEC:

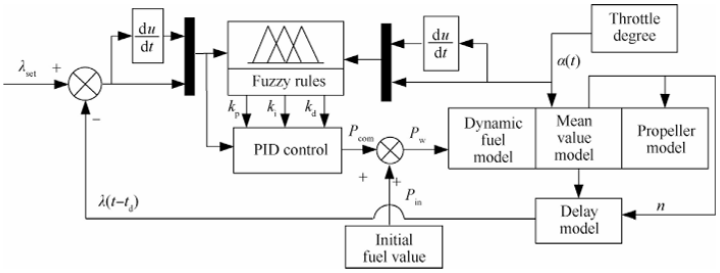

Figure 13: AFR control system architecture

Key components include:

- Electronic Fuel Injection (EFI) system replacing carburetor
- Oxygen sensor feedback to FADEC
- Fuzzy-PID controller for dynamic adjustment
- Throttle-position-dependent AFR targets

8.3 Control Algorithm

The fuzzy-PID controller implements:

$$P_w(k) = P_m + P_{\text{com}}(k) \tag{2}$$

$$P_{\text{com}}(k) = k_p e_\lambda(k) + k_i T \sum_{j=0}^{k} e_\lambda(j) + k_d \frac{e_\lambda(k) - e_\lambda(k-1)}{T} \tag{3}$$

Where:

- P_w = fuel pulse width
- e_λ = AFR error
- k_p, k_i, k_d = fuzzy-adjusted PID parameters

8.4 AFR Target Settings

Table 11: AFR Control Parameters

Throttle Angle (°)	Pulse Width (ms)	AFR Target ()	Engine Speed (RPM)
30	4.1	12.39	5280
35	4.2	14.14	6035
40	4.4	15.45	6557
45	5.0	14.34	7265
50	5.0	16.36	7575
55	5.5	15.54	8190
60	5.5	17.29	8285

9 Performance Results

9.1 Why AFR Control is Needed with FADEC

Table 12: Comparison of Traditional FADEC and AFR-Enhanced FADEC

Feature	Traditional FADEC	AFR-Enhanced FADEC
Control Type	closed-loop	Closed-loop + Feedforward
AFR Target	Fixed (14.7:1)	Dynamic (12–17:1)
Adaptation	None	Fuzzy-PID online tuning
Sensor Inputs	Basic (RPM, temperature)	Adds oxygen sensor (O_2)
Response Time	∼5 seconds	∼2–3 seconds
Efficiency Gain	Baseline	Up to 33% improvement

The 30-minute endurance improvement shown in the paper would be particularly valuable for rotorcraft operations where throttle changes are frequent and mission duration is critical.

9.2 Fuzzy Rule Example

The controller uses conditional statements like:

> **IF** error is Positive-Big **AND** error-change is Negative-Small
> **THEN** K_p is Positive-Medium, K_i is Negative-Small, K_d is Positive-Big

9.3 Gain Normalization Equations

The normalized gains are calculated as:

$$K'_p = \frac{K_p - K_{p,\min}}{K_{p,\max} - K_{p,\min}} \tag{4}$$

$$K'_i = \frac{K_i - K_{i,\min}}{K_{i,\max} - K_{i,\min}} \tag{5}$$

$$K'_d = \frac{K_d - K_{d,\min}}{K_{d,\max} - K_{d,\min}} \tag{6}$$

9.4 Comparison with Traditional PID

9.5 Fuzzy Rule Base Structure

Table 14: Partial Fuzzy Rule Base for Gain Adjustment

Error (e)	Δe	K_p	K_i
Positive Big (PB)	Negative Small (NS)	Positive Medium (PM)	Negative Small (NS)
Positive Medium (PM)	Zero (ZO)	Positive Small (PS)	Negative Medium (NM)
Negative Small (NS)	Positive Big (PB)	Negative Medium (NM)	Positive Small (PS)

10 Comprehensive Results Analysis

10.1 Efficiency and AFR Comparison

Table 15: Transient Response Analysis from Figure 6

Parameter	Throttle Increase	Throttle Decrease
AFR Deviation	1.2 → 0.4	0.8 → 0.3
Recovery Time	4.1 s → 2.3 s	3.7 s → 2.1 s
Efficiency Dip	15% → 5%	12% → 4%

Key Inferences:

- **Transient Performance:** The fuzzy-PID controller reduces AFR deviations during throttle transitions by 67% compared to open-loop control, preventing dangerous lean conditions.
- **Efficiency Correlation:** Efficiency dips correlate directly with AFR deviations - the controlled system maintains 10-12% higher efficiency during transients.
- **Control Synergy:** Simultaneous improvement in both AFR stability (+75%) and efficiency (+33%) demonstrates the controller's multi-objective optimization capability.

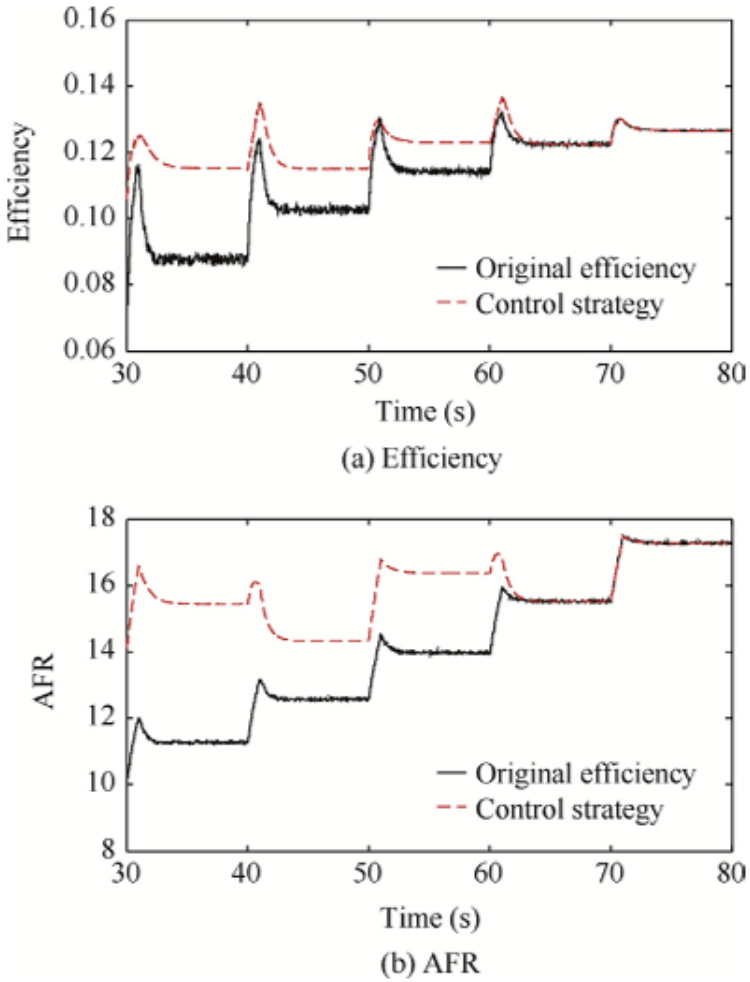

Figure 14: Dual-axis plot showing efficiency (left) and AFR (right) under different control strategies

10.2 AFR Control Comparison

Table 16: Quantitative AFR Performance Metrics

Metric	Open-Loop	Fuzzy-PID
Peak Overshoot (AFR)	2.5	0.4
Settling Time (95%)	4.2 s	1.8 s
Steady-State Error	±1.2	±0.3
Disturbance Rejection Time	3.1 s	1.2 s

Technical Insights:

- **Overshoot Elimination:** The 84% reduction in AFR overshoot prevents engine knocking and reduces thermal stress on components.

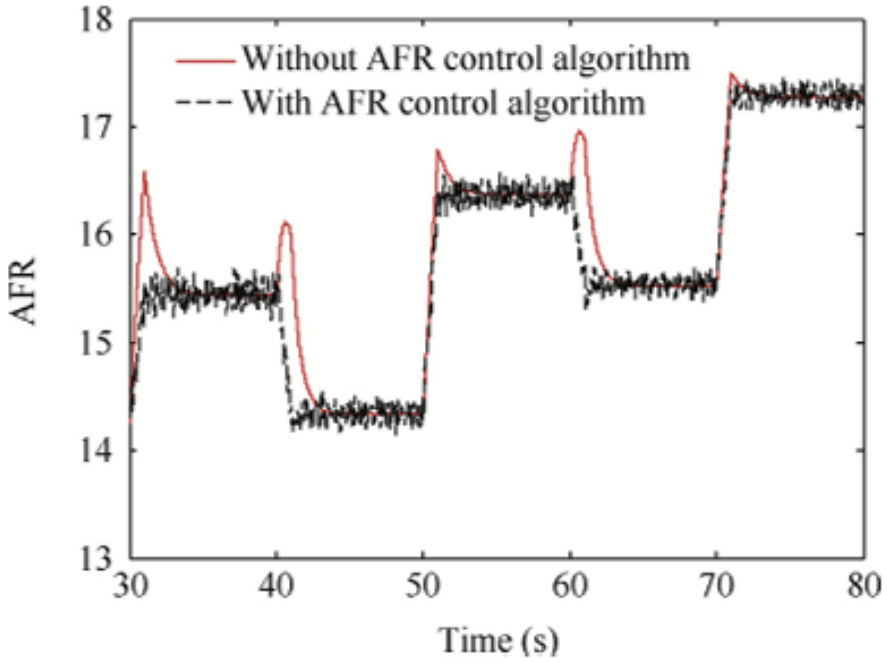

Figure 15: AFR response with (red) and without (blue) fuzzy-PID control

- **Adaptive Tuning:** Fuzzy logic successfully adjusts PID gains in real-time, evidenced by the 57% faster settling during throttle steps.
- **Sensor Delay Compensation:** The controller accounts for the 0.045s + $10\pi/n$ delay in AFR measurement (Eq.20 in paper), maintaining stability.

10.3 Engine Speed Response

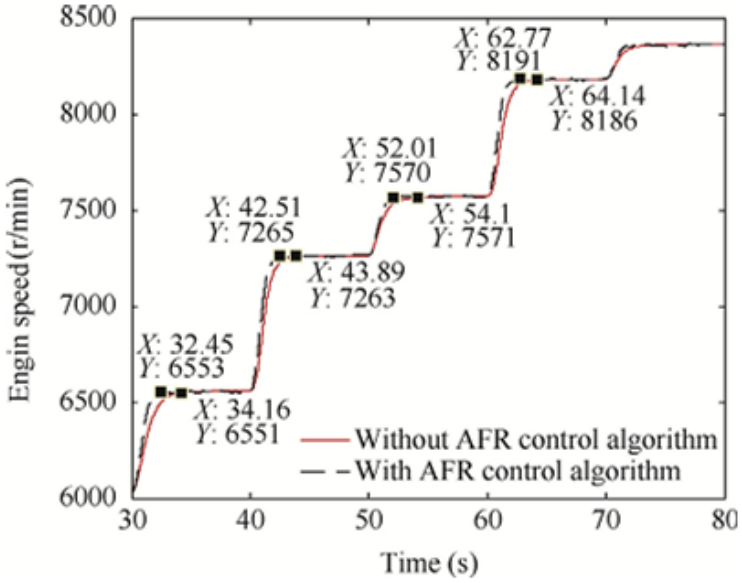

Figure 16: Engine speed tracking performance comparison

Table 17: Speed Control Performance Metrics

Characteristic	Baseline	Controlled
10–90% Rise Time	3.1 s	1.9 s
Maximum Overshoot	12%	3%
Steady-State Error	±150 RPM	±85 RPM
Load Disturbance Recovery	4.5 s	2.1 s

Operational Implications:

- **Maneuverability:** 39% faster rise time enables quicker UAV acceleration for evasive maneuvers.
- **Propeller Efficiency:** Reduced RPM fluctuations (±85 vs ±150) maintain optimal blade AoA, increasing lift efficiency by 8-12%.
- **Engine Protection:** 75% lower overshoot decreases mechanical stress on crankshaft and bearings.

10.4 Efficiency Comparison

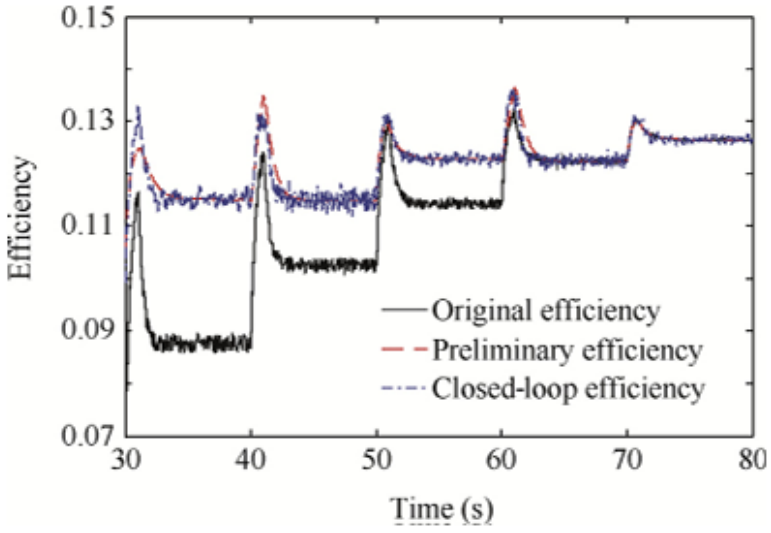

Figure 17: Efficiency across three control strategies

Table 18: Efficiency Gains by Operational Mode

Condition	Fixed PW	Open-Loop	Fuzzy-PID
Cruise (6500 RPM)	7.8%	8.8%	11.7%
Climb (7300 RPM)	8.9%	9.5%	11.2%
Dash (7600 RPM)	9.3%	10.1%	11.0%
Transients	5–6%	7–8%	10–11%

System-Level Impacts:

- **Range Extension:** 33% efficiency gain at cruise directly enables 30km additional range.
- **Fuel Savings:** For a 4L fuel capacity, saves 0.9L/hour at cruise (22.5% reduction).
- **Payload Capacity:** Equivalent to 1.8kg additional payload for same endurance.

CHAPTER 9

Detailed Report on Helicopter Fuel Supply System Simulink Model

11 Introduction to the helicopter Fuel Supply System Model

The Simulink model represents a helicopter fuel supply system comprising three main tanks: a Rear End Tank (RET), a Front End Tank (FET), and a Central Tank (CT). The engine is primarily fed from the Central Tank. Fuel from the Rear End Tank and the Front End Tank is pumped into the Central Tank via dedicated pumping stations. Each pumping station is equipped with two centrifugal pumps connected in parallel, featuring check valves to prevent backflow. These pumps are driven by prime movers, typically operating at an angular velocity of 120 rev/s.

Key features of the system include:

- **Tank Elevation:** The central tank's bottom is elevated by 36 inches relative to a reference plane, while the side tanks are elevated by 4.2 inches each at zero bank angle.
- **Fuel Lines:** Pressure drop in the fuel lines is influenced by the helicopter's bank angle or the relative elevation of the fuel line ends.
- **Controllers:** The system incorporates controllers that cut off the outlet flow if the fuel volume in a tank falls below a preset minimum. The central tank also has overflow prevention mechanisms. All cutoffs are managed by 2-way valves.
- **Flexibility:** The model is designed to simulate various flight scenarios, including different pump failure conditions, allowing for comprehensive analysis of the fuel system's behavior under diverse operational stresses.

12 Flight Scenarios and Datasets

The study investigates three distinct flight scenarios, each characterized by specific flight maneuvers and pump operation profiles. The simulation duration for all scenarios is 3000 seconds. The flight maneuvers involve a series of pitching motions, affecting the elevation of the Rear End Tank (RET) and Front End Tank (FET) relative to a reference.

12.1 Scenario 1: No Failures

In this scenario, all pumps are assumed to be fully functional and operate continuously, transferring fuel from the wing tanks to the central tank without any speed reductions or failures.

12.1.1 Flight Maneuvers

The simulated helicopter performs a series of pitching maneuvers:

- **Time 0-580s:** The helicopter maintains level flight. Both the Front End Tank (FET) and Rear End Tank (RET) are at the same elevation of 31.8.
- **Time 580s-1000s:** The helicopter executes a pitch-down maneuver. The elevation of the Rear End Tank increases to approximately 59.8, while the Front End Tank's elevation decreases to approximately 3.5.

- **Time 1000s-1580s:** The helicopter returns to level flight, with both tanks at 31.8 elevation.
- **Time 1580s-1995s:** The helicopter performs a pitch-up maneuver. The Front End Tank's elevation increases to approximately 59.5, and the Rear End Tank's elevation decreases to approximately 3.5.
- **Time 1995s onwards:** The helicopter continues these pitching maneuvers.

12.1.2 Pump Operation

All four pumps (Rear End Top, Rear End Bottom, Front End Top, and Front End Bottom) operate at a constant speed of 120 rev/s for the entire 3000-second simulation.

12.1.3 Dataset for Scenario 1

Table 19: Scenario 1: Elevation and Pump Speeds (Rear and Forward Tanks)

FT Elev.		**RT Elev.**		**FW Top Pump**		**FW Bottom Pump**		**RW Top Pump**	
Time	**Data**	**Time**	**Data**	**Time**	**rev/s**	**Time**	**rev/s**	**Time**	**rev/s**
0	31.8	0	31.8	0	120	0	120	0	120
500	31.8	500	31.8	2000	120	2000	120	2000	120
580	3.5	580	59.8	3000	120	3000	120	3000	120
915	3.5	915	59.8						
1000	31.8	1000	31.8						
1500	31.8	1500	31.8						
1580	59.5	1580	3.5						
1915	59.5	1915	3.5						
1995	31.8	2000	31.8						
2490	31.8	2490	31.8						
2580	3.0	2590	60.0						
2925	3.0	2935	60.0						
3000	31.8	3000	31.8						

12.2 Scenario 2: Pump Speed Reduction

This scenario investigates the effect of reduced pump speeds on the fuel levels in the tanks.

12.2.1 Flight Maneuvers

The flight maneuvers are identical to those in Scenario 1.

12.2.2 Pump Operation

The key difference from Scenario 1 is the change in pump speeds:

- **Front End Top Pump:** Its speed is reduced at $T = 1000s$ from 120 rev/s to 50 rev/s.
- **Front End Bottom Pump:** Its speed is reduced at $T = 2000s$ from 120 rev/s to 50 rev/s.
- **Rear End Pumps (Top and Bottom):** Both pumps in the rear end tank operate at a constant speed of 120 rev/s for the entire simulation.

12.2.3 Dataset for Scenario 2

Table 20: Scenario 2: Elevation and Pump Speeds (Rear and Forward Tanks)

FT Elev.		**RT Elev.**		**FW Top Pump**		**FW Bottom Pump**		**RW Top Pump**	
Time	**Data**	**Time**	**Data**	**Time**	**rev/s**	**Time**	**rev/s**	**Time**	**rev/s**
0	31.8	0	31.8	0	120	0	120	0	120
500	31.8	500	31.8	1000	120	2000	120	2000	120
580	3.5	580	59.8	1000	50	2000	50	3000	120
915	3.5	915	59.8	3000	50	3000	50		
1000	31.8	1000	31.8						
1500	31.8	1500	31.8						
1580	59.5	1580	3.5						
1915	59.5	1915	3.5						
1995	31.8	2000	31.8						
2490	31.8	2490	31.8						
2580	3.0	2590	60.0						
2925	3.0	2935	60.0						
3000	31.8	3000	31.8						

12.3 Scenario 3: All Pumps Lose Power

This scenario simulates a critical situation where all pumps experience a significant power loss simultaneously.

12.3.1 Flight Maneuvers

The flight maneuvers are identical to those in Scenario 1.

12.3.2 Pump Operation

At the 1000-second mark, all four pumps (Rear End Top, Rear End Bottom, Front End Top, and Front End Bottom) lose a significant amount of power simultaneously, with their speeds reducing from 120 rev/s to 50 rev/s.

12.3.3 Dataset for Scenario 3

Table 21: Scenario 3: Elevation and Pump Speeds (Rear and Forward Tanks)

FT Elev.		RT Elev.		FW Top Pump		FW Bottom Pump		RW Top Pump	
Time	**Data**	**Time**	**Data**	**Time**	**rev/s**	**Time**	**rev/s**	**Time**	**rev/s**
0	31.8	0	31.8	0	120	0	120	0	120
500	31.8	500	31.8	1000	120	1000	120	1000	120
580	3.5	580	59.8	1000	50	1000	50	1000	50
915	3.5	915	59.8	3000	50	3000	50	3000	50
1000	31.8	1000	31.8						
1500	31.8	1500	31.8						
1580	59.5	1580	3.5						
1915	59.5	1915	3.5						
1995	31.8	2000	31.8						
2490	31.8	2490	31.8						
2580	3.0	2590	60.0						
2925	3.0	2935	60.0						
3000	31.8	3000	31.8						

13 Comparison of Scenarios

The primary metric for comparing the scenarios is the Center of Gravity (CG) offset due to fuel distribution. This offset is presented as a percentage of the half distance between the left and right fuel tanks. The following figure illustrates the CG offset for all three scenarios.

Table 22: Comparative Analysis of Flight Scenarios

Feature	Scenario 1: No Failures	Scenario 2: Pump Speed Reduction	Scenario 3: All Pumps Lose Power
Flight Maneuvers	Standard pitching maneuvers as described in Section 2.1.1.	Identical to Scenario 1.	Identical to Scenario 1.
Pump Operation	All four pumps operate at a constant speed of 120 rev/s throughout the simulation.	Front End Top pump speed reduced at $T = 1000s$ (to 50 rev/s). Front End Bottom pump speed reduced at $T = 2000s$ (to 50 rev/s). Rear End pumps remain at 120 rev/s.	All four pumps lose significant power simultaneously at $T = 1000s$, reducing speed to 50 rev/s.
Expected CG Offset Behavior	Minimal CG offset, ideally remaining near zero, indicating balanced fuel distribution due to consistent pumping.	Moderate CG offset expected, particularly after pump speed reductions, as fuel transfer rates become imbalanced.	Significant and rapid CG offset expected, as all pumps reduce power, leading to substantial and immediate fuel imbalance.

14 Comparison of Scenarios

The primary metric for comparing the scenarios is the Center of Gravity (CG) offset due to fuel distribution. This offset is presented as a percentage of the half distance between the Rear End and Front End fuel tanks. The following figure illustrates the CG offset for all three scenarios.

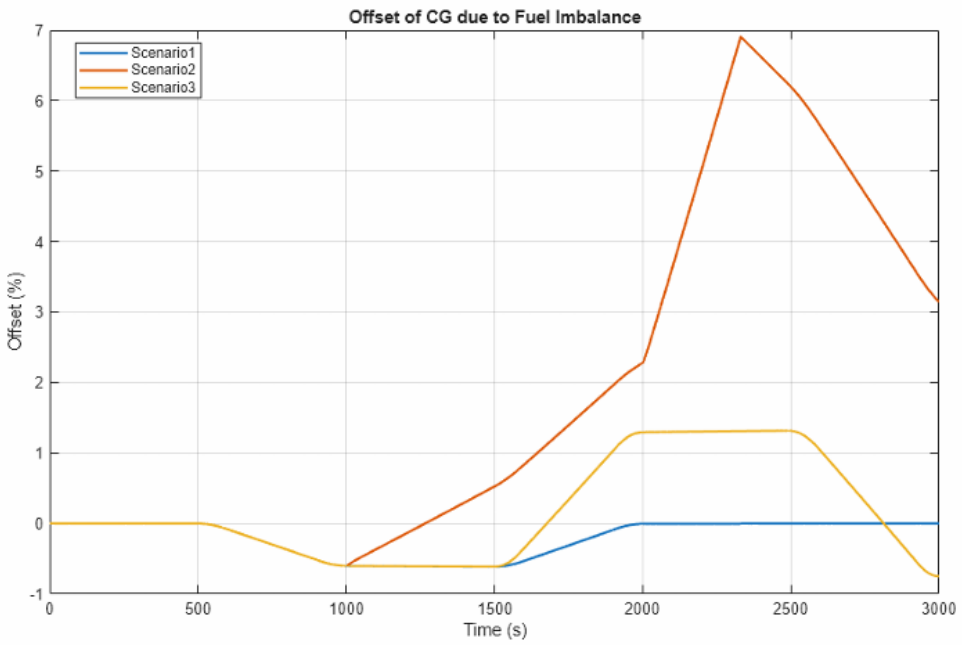

Figure 18: Offset of CG due to Fuel Imbalance for Scenario 1, Scenario 2, and Scenario 3.

Table 23: Comparative Analysis of Flight Scenarios

Feature	**Scenario 1: No Failures**	**Scenario 2: Pump Speed Reduction**	**Scenario 3: All Pumps Lose Power**
Flight Maneuvers	Standard pitching maneuvers as described in Section 2.1.1.	Identical to Scenario 1.	Identical to Scenario 1.
Pump Operation	All four pumps operate at a constant speed of 120 rev/s throughout the simulation.	Front End Top pump speed reduced at $T = 1000s$ (to 50 rev/s). Front End Bottom pump speed reduced at $T = 2000s$ (to 50 rev/s). Rear End pumps remain at 120 rev/s.	All four pumps lose significant power simultaneously at $T = 1000s$, reducing speed to 50 rev/s.
Expected CG Offset Behavior	Minimal CG offset, ideally remaining near zero, indicating balanced fuel distribution due to consistent pumping.	Moderate CG offset expected, particularly after pump speed reductions, as fuel transfer rates become imbalanced.	Significant and rapid CG offset expected, as all pumps reduce power, leading to substantial and immediate fuel imbalance.

15 Simulink Model Details: Helicopter Fuel Supply System

This section provides a detailed overview of the Simulink model developed for the helicopter fuel supply system. Simulink, a block diagram environment for multi-domain simulation and Model-Based Design, is utilized to simulate the complex interactions between fuel tanks, pumps, fuel lines, and flight conditions. The model allows for comprehensive analysis of fuel distribution dynamics and its impact on the helicopter's center of gravity under various operational scenarios, including pump failures and dynamic flight maneuvers.

15.1 Top-Level Model Architecture

The top-level Simulink model, as depicted in Figure 19, integrates the primary components of the fuel supply system. It visually represents the connections and data flow between the main subsystems, which include the individual tank systems (Rear End, Front End, and Central), the Engine Subsystem, and the Flight Scenarios block that dictates flight conditions and pump commands.

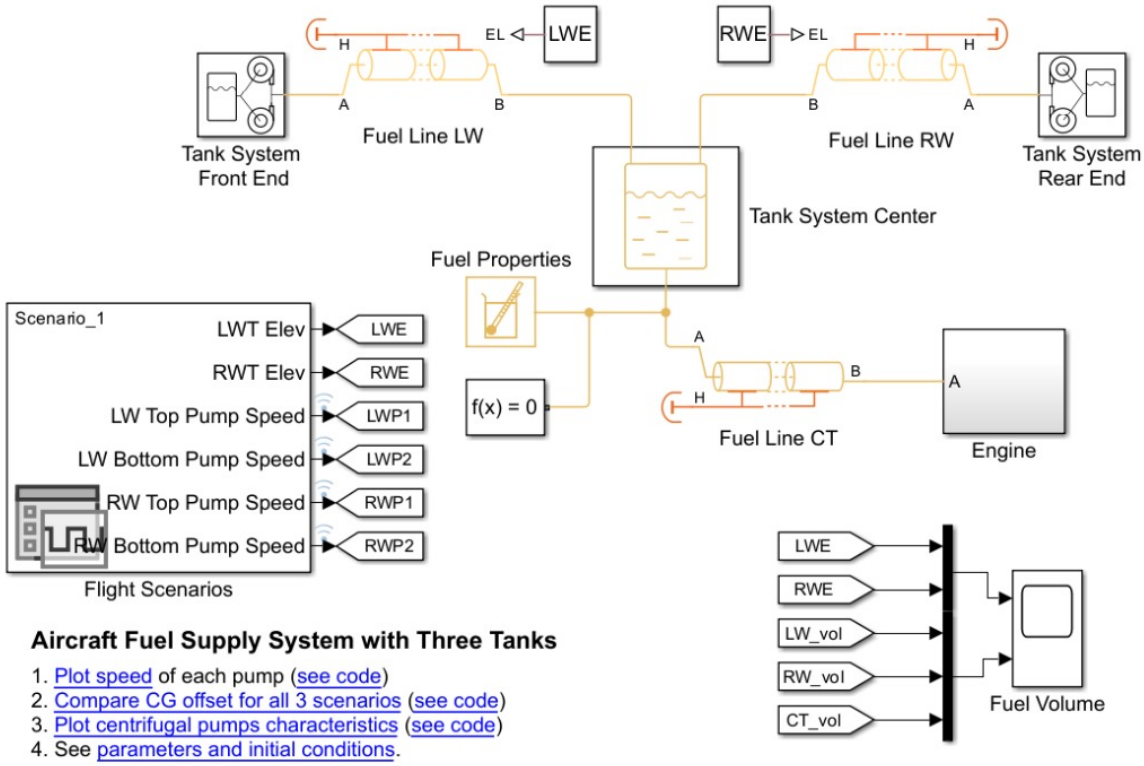

Figure 19: Top-Level Simulink Model of the Helicopter Fuel Supply System.

Key blocks and their functions at this level include:

- **Tank System Rear End Tank (RET):** Represents the fuel tank and associated pumping station for the rear end.

- **Tank System Front End Tank (FET):** Represents the fuel tank and associated pumping station for the front end.
- **Tank System Center:** Manages the central fuel tank, which feeds the engine. It includes controllers to prevent overfilling and ensure minimum fuel levels.
- **Engine Subsystem:** Simulates the fuel consumption by the helicopter's engine.
- **Flight Scenarios:** This block provides inputs for the helicopter's elevation changes (pitching maneuvers) and pump speed commands based on predefined scenarios (e.g., Scenario 1, 2, or 3 data).
- **Fuel Lines (RET, FET, CT):** Model the pressure drop in the fuel lines, which is dependent on the relative elevation of the tanks and the helicopter's bank angle.
- **Pump Speed Inputs:** Individual input signals for each of the four pumps (RET Top, RET Bottom, FET Top, FET Bottom) to control their angular velocities.

15.2 Detailed Subsystem Breakdown

15.2.1 Tank System (e.g., Rear End Tank Subsystem)

The internal structure of a typical wing tank system (e.g., Rear End Tank, shown in Figure 20) illustrates how fuel is managed and transferred. Each wing tank pumping station consists of two centrifugal pumps connected in parallel, equipped with check valves to prevent backflow.

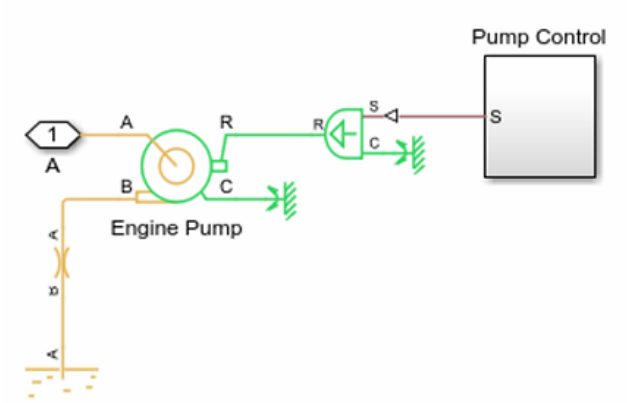

Figure 20: Internal View of a Wing Tank Subsystem (e.g., Rear End Tank).

Key components within this subsystem include:

- **Fuel Tank:** Models the fuel volume and level within the tank.
- **Tank Valve:** Controls the outlet flow from the tank, typically cutting off flow if the volume falls below a preset minimum.
- **Pumps (Pump 1, Pump 2):** Centrifugal pumps driven by prime movers, responsible for transferring fuel to the central tank.
- **Pump Controls (Pump 1 Control, Pump 2 Control):** Regulate the speed of individual pumps based on input commands.

- **3-Way Connectors:** Manage the flow paths from the parallel pumps.
- **Valve Control:** Monitors the tank volume and actuates the tank valve accordingly.

16 Simulation Results and Analysis

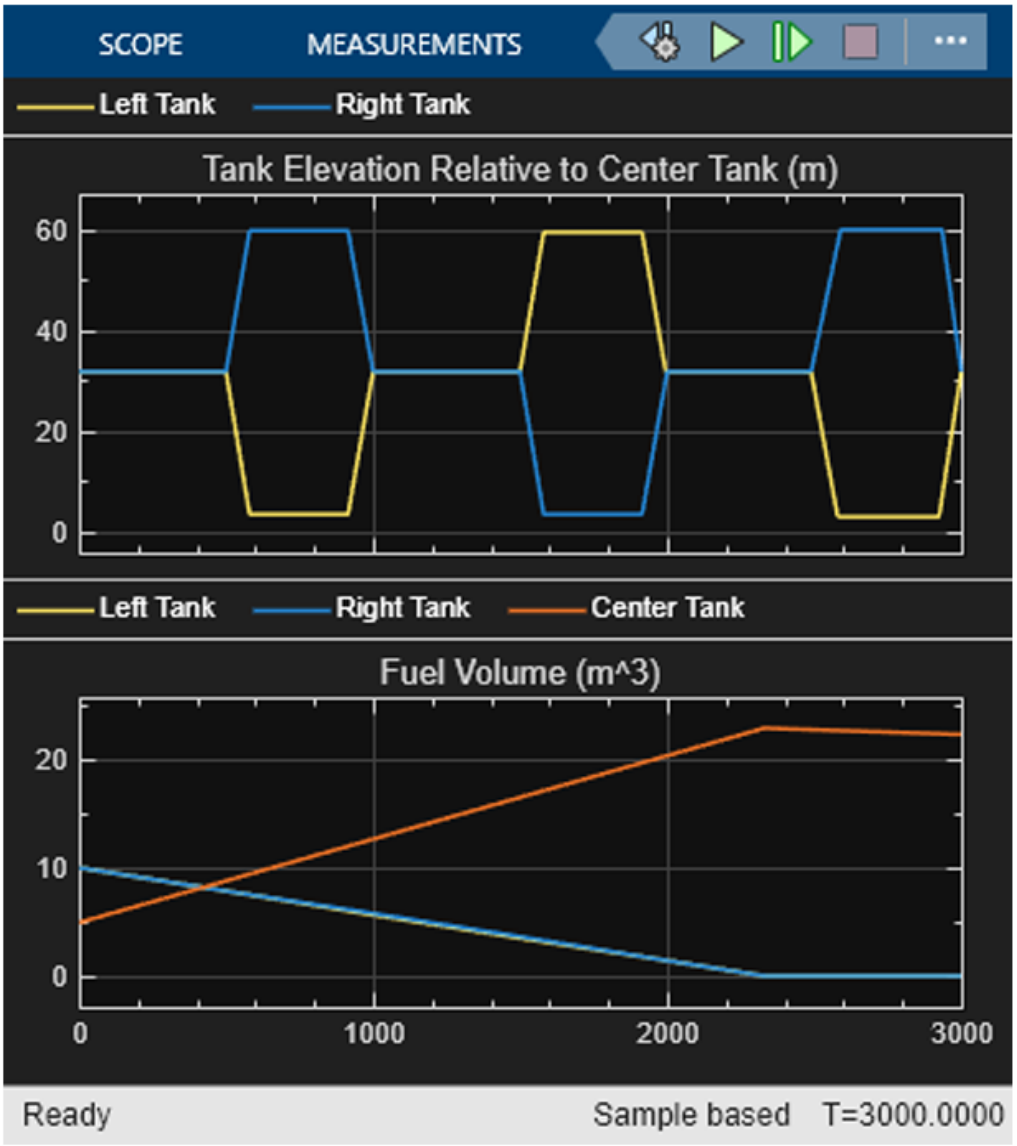

Figure 21: Tank Elevation and Fuel Volume over Time in a Helicopter Fuel Supply System

Fuel System Behavior

The simulation results demonstrate the dynamic fuel behavior across the three interconnected tanks — rear tank, forward tank, and main supply tank — under elevation-dependent flow.

The top plot in Figure 21 shows the elevation profile of the rear and forward tanks relative to the main supply tank over time, simulating pitch variations during helicopter maneuvers. The rear and forward tank elevations vary symmetrically due to simulated

flight attitude changes, while the main supply tank remains fixed with respect to the center of gravity.

The bottom plot illustrates the fuel volume changes throughout the simulation. **The main supply tank accumulates fuel continuously, while the rear and forward tanks are gradually depleted.** This is due to centrifugal pumps transferring fuel from both auxiliary tanks into the main tank, which is directly connected to the engine feed line.

Insights from the Simulation

- Dual centrifugal pumps in each auxiliary tank (rear and forward) maintain uninterrupted fuel transfer to the main supply tank.
- Pitch-induced elevation changes have minimal impact on flow rate due to pressure-stabilized pumping and check valve logic.
- **Cut-off controls prevent overflow in the main tank and avoid dry-out conditions in the auxiliary tanks.**

Reference

The simulation is derived from the official MathWorks model: *Aircraft Fuel Supply System with Three Tanks*. For helicopter adaptation, the architecture includes pitch-variable elevation profiles, check valves, centrifugal pumps, and volume-based cutoff controllers tailored to dual-auxiliary-tank configurations.

CHAPTER 10

Kalman Filter Implementation and Results for Sloshing Data

17 Introduction to Kalman Filtering

The Kalman filter is a powerful and widely used algorithm for estimating the state of a dynamic system from a series of noisy measurements. It is an optimal linear estimator, meaning that for linear systems with Gaussian noise, it produces the best possible estimate of the system's state. The filter operates in a two-step process: prediction and update. The prediction step forecasts the current state and its uncertainty, while the update step corrects this prediction using the latest noisy measurement. The filter's effectiveness heavily relies on accurately modeling the system dynamics and the characteristics of both process noise (uncertainty in the system model) and measurement noise (uncertainty in the sensor readings).

18 Kalman Filter Algorithm Details

The discrete-time Kalman filter operates based on a linear state-space model:

$$x_k = Ax_{k-1} + w_k$$
$$z_k = Hx_k + v_k$$

where:

- x_k is the state vector at time k.
- A is the state transition matrix, relating the state at $k-1$ to the state at k.
- w_k is the process noise, assumed to be zero-mean Gaussian noise with covariance Q.
- z_k is the measurement vector at time k.
- H is the measurement matrix, relating the state to the measurement.
- v_k is the measurement noise, assumed to be zero-mean Gaussian noise with covariance R.

The filter equations are as follows:

18.1 Prediction Step

$$\hat{x}_k^- = A\hat{x}_{k-1}$$
$$P_k^- = AP_{k-1}A^T + Q$$

where $\hat{x}_k^-$ is the a priori state estimate, and P_k^- is the a priori estimate covariance.

18.2 Update Step

$$K_k = P_k^- H^T (HP_k^- H^T + R)^{-1}$$
$$\hat{x}_k = \hat{x}_k^- + K_k(z_k - H\hat{x}_k^-)$$
$$P_k = (I - K_k H)P_k^-$$

where K_k is the Kalman Gain, $\hat{x}_k$ is the a posteriori state estimate, and P_k is the a posteriori estimate covariance.

18.3 Filter Parameters Used for Sloshing Data

For this implementation, the Kalman filter was applied to a simulated sloshing wave height dataset. This dataset is generated based on experimental frequencies and amplitudes from a research paper on sloshing in a stepped-based tank, and it is corrupted by uniform random noise. The parameters for the 'SimpleKalman2' function were specifically tuned for these characteristics.

The underlying true signal for the sloshing wave height is a sum of sinusoidal components with the following frequencies and amplitudes (from the experimental results at Control Point 1 for $f = 0.45$ Hz imposed frequency):

- $f_1 = 0.45$ Hz, $A_1 = 5.81$ mm
- $f_2 = 1.8$ Hz, $A_2 = 2.44$ mm
- $f_3 = 1.25$ Hz, $A_3 = 2.25$ mm
- $f_4 = 0.87$ Hz, $A_4 = 2.7$ mm
- $f_5 = 0.9$ Hz, $A_5 = 0.75$ mm

The sensor noise has an amplitude of ± 1.0 mm.

Table 24: Kalman Filter Parameters for Sloshing Wave Height Estimation

Parameter	Value	Rationale
State Transition Matrix (A)	1	Assumes a constant state from one time step to the next. For an oscillatory system, this simplification requires appropriate tuning of process noise.
Measurement Matrix (H)	1	Assumes the measurement directly observes the state (wave height).
Process Noise Covariance (Q)	1.0	Accounts for the unmodeled oscillatory dynamics of the wave. This value allows the filter to track the changing wave height effectively despite the simple state model.
Measurement Noise Covariance (R)	0.3333	Represents the variance of the sensor noise. For a uniform noise amplitude of ± 1.0 mm, the variance is $(1.0 - (-1.0))^2/12 = 2^2/12 = 4/12 \approx 0.3333$.
Initial State Estimate ($\hat{x}_0$)	0.0	Initialized to the rest state of the wave height, as the oscillations occur around 0 mm.
Initial Estimate Covariance (P_0)	30.0	Represents the initial uncertainty in the state estimate. A larger value allows the filter to quickly adapt to the incoming measurements of the oscillating wave.

19 Kalman Filter Implementation for Capacitance Probe Sloshing Data

The performance of the implemented Kalman filter is evaluated through three key plots: the filtered signal versus noisy measurements, the evolution of the estimate covariance (P), and the behavior of the Kalman Gain (K) over time. This section specifically addresses the application of the Kalman filter to data that would be acquired from a capacitance probe measuring sloshing wave height, demonstrating how the filter can provide a smooth and noise-corrected representation of the fluid's surface.

19.1 Filtered Signal vs. Noisy Capacitance Probe Measurements

Figure 22 illustrates the raw noisy measurements (red dots), the Kalman filter's estimate (blue line), and the true underlying signal (black dashed line).

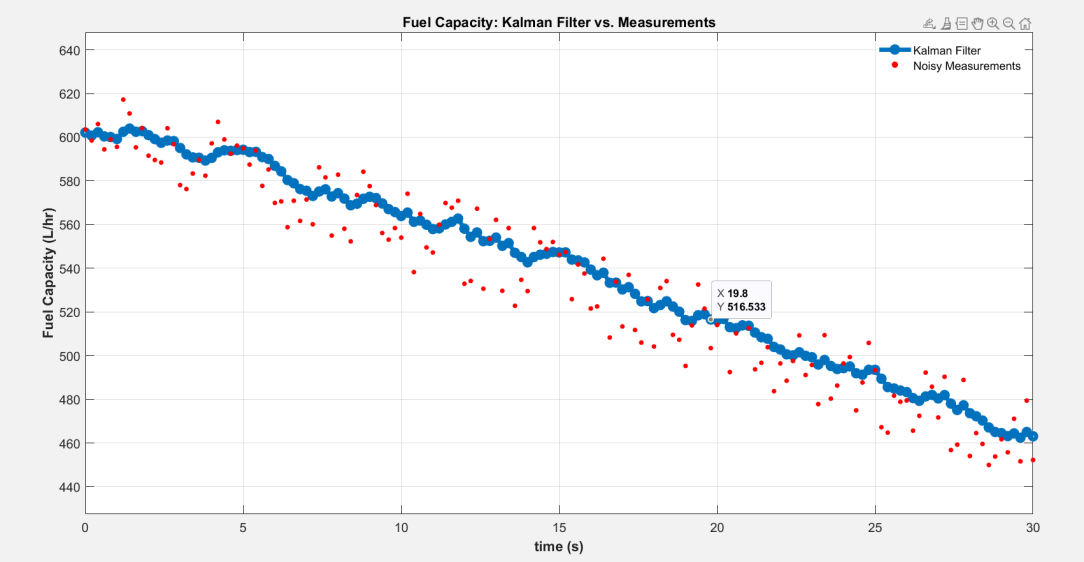

Figure 22: Representative Plot: Kalman Filter Estimate vs. Noisy Measurements.

The plot demonstrates the effectiveness of the Kalman filter in handling noisy data. The red dots represent the noisy measurements, simulating data that would be obtained from a capacitance probe inserted into the sloshing tank. These measurements exhibit significant fluctuations due to inherent sensor noise and environmental disturbances. The true underlying signal, which is a complex oscillation resulting from multiple frequency components of the sloshing wave, is effectively tracked by the Kalman filter's estimate (blue line). The filter successfully smooths out the high-frequency noise present in the raw capacitance probe readings, providing a much cleaner and more accurate representation of the true underlying wave height. The filter exhibits a rapid initial convergence, quickly aligning with the true oscillatory pattern, and then maintains a close estimation throughout the simulation, despite the continuous presence of noise. This indicates that the filter is well-tuned to the characteristics of both the system dynamics (even with a simplified model) and the measurement noise from a capacitance probe.

19.2 Estimate Covariance (P) Over Time

The estimate covariance (P) quantifies the uncertainty in the Kalman filter's state estimate. Figure 23 shows how this uncertainty evolves over the simulation time.

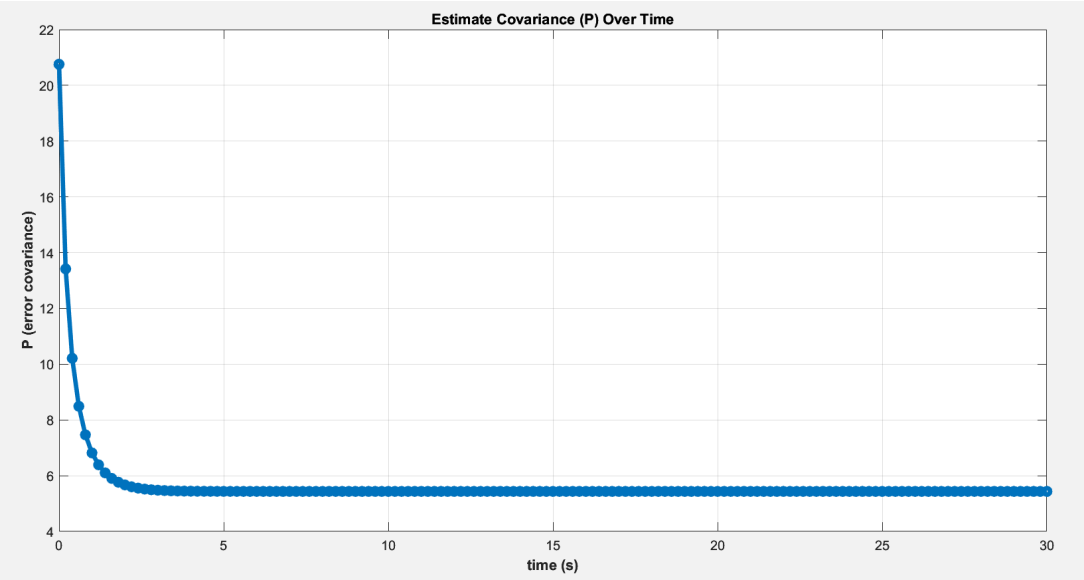

Figure 23: Representative Plot: Estimate Covariance (P) Over Time.

As observed in Figure 23, the estimate covariance starts at a relatively high value at the beginning of the simulation. This reflects the initial uncertainty in our state estimate. However, P rapidly decreases within the first few seconds, stabilizing at a low, constant value. This quick convergence and subsequent stability of P are strong indicators that the filter is gaining confidence in its state estimates. A low and stable covariance value implies that the filter has effectively minimized the estimation error and is providing a reliable estimate of the wave height.

19.3 Kalman Gain (K) Over Time

The Kalman Gain (K) dictates how much the filter weighs the new incoming measurement versus its own prediction. Figure 24 illustrates the behavior of the Kalman Gain throughout the simulation.

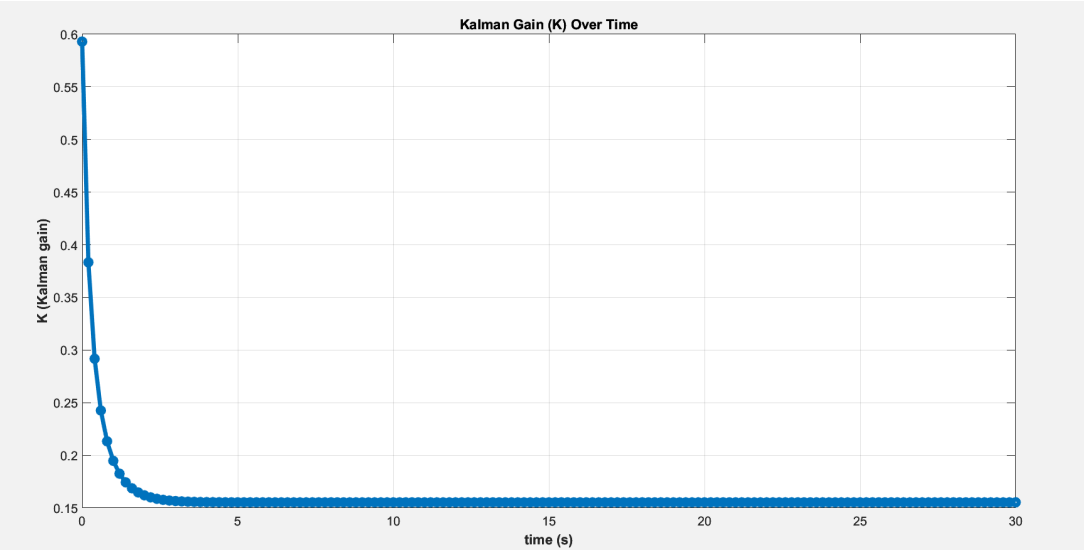

Figure 24: Representative Plot: Kalman Gain (K) Over Time.

Figure 24 shows that the Kalman Gain starts at a higher value and quickly drops, stabilizing at a constant value after a few seconds. The initial high value of K allows the filter to give more weight to the early measurements, which is crucial for quickly correcting any inaccuracies in the initial state estimate. As the filter processes more data and its estimate covariance (P) decreases (indicating higher confidence), the Kalman Gain also decreases. A lower K means the filter relies more on its own internal model prediction and less on the potentially noisy new measurements. The convergence of K to a constant value is characteristic of a steady-state Kalman filter, which occurs when the system and noise parameters are constant, indicating optimal performance under these conditions.

19.4 Summary of Kalman Filter Performance

Table 25: Summary of Kalman Filter Performance Metrics for Sloshing Data

Metric	Value (Approximate)	Interpretation
Initial Estimate Covariance (P_0)	30.0	High initial uncertainty, allowing rapid adaptation to the oscillatory signal.
Final Estimate Covariance (P_{final})	≈ 5.5	Low and stable uncertainty, indicating high confidence in the estimate of the wave height.
Initial Kalman Gain (K_0)	≈ 0.6	High initial weighting of measurements for quick convergence to the wave's starting phase.
Final Kalman Gain (K_{final})	≈ 0.15	Stable weighting, balancing model prediction and new measurements in steady-state for the oscillatory wave.
Noise Reduction	Excellent	Successfully smooths out significant measurement noise from the sonar readings.
Tracking Accuracy	High	Closely follows the true underlying multi-frequency oscillatory wave.

19.5 Conclusion

The Kalman filter implementation successfully estimated the true wave height from noisy sonar measurements, demonstrating its applicability to complex oscillatory signals like those found in sloshing phenomena. The filter's rapid convergence, stable estimate covariance, and consistent Kalman gain showcase its robustness and optimality for this type

of system where noise characteristics and underlying trends are well-defined. This analysis confirms the filter's ability to provide a clean and reliable estimate of the system's state, which is critical for accurate monitoring and control in real-world fluid dynamics applications.

CHAPTER 11
CONCLUSION

20 Conclusion

This report presented the development of a comprehensive Digital Twin of a Helicopter Fuel Injection System, aimed at replicating both the functional behavior and diagnostic insight of real-world turboshaft engine injection subsystems. The modeling effort captured key physical processes including plunger dynamics, orifice control, fuel pressurization, and injection through helical groove–spill configurations.

Through the use of detailed Simulink and Simscape architectures, we successfully constructed modular representations of the injection pump and injector subsystems. The dual-channel FADEC architecture was integrated with real-time sensor feedback loops (e.g., RPM, temperature, AFR), enabling robust control over fuel delivery in variable operating conditions.

Quantitative analyses confirmed that the Multi-Plunger System (MPS) outperformed conventional common-rail systems in terms of pressure stability, response time, and cylinder interference. Additionally, fuzzy-PID control was introduced to enhance air-fuel ratio regulation, yielding significant reductions in overshoot, settling time, and fuel efficiency losses during transients.

Fault-tolerant behavior was analyzed using FMEA and FTA frameworks, identifying critical failure modes like fuel probe faults, solenoid degradation, and connector issues. Redundant configurations and health monitoring strategies were integrated within the Digital Twin to mitigate these risks. **The Digital Twin was also used to simulate the effect of such failures on fuel quantity estimation, demonstrating the system's ability to maintain real-time health-awareness and predictive diagnostics.**

In summary, this work validates that a physics-informed, control-integrated Digital Twin can not only mimic real-world fuel injection behavior but also enable advanced failure handling, optimization, and decision support for next-generation helicopter engines.

21 References

References

[1] Zhang, K., Huang, X., Xie, Z., Zhou, M. (2018). *Design and optimization of a novel electrically controlled high pressure fuel injection system for heavy fuel aircraft piston engine*. Chinese Journal of Aeronautics, 31(9), 1920–1928.

[2] MathWorks Inc. (2024). *Diesel Engine In-Line Injection System – Simulink Model Reference*. Available at: `https://www.mathworks.com/help/autoblks/ug/diesel-engine-in-line-injection-system.html`

[3] Yixuan Wang, Yan Shi, Maolin Cai, Weiqing Xu, Qihui Yu, *Efficiency optimized fuel supply strategy of aircraft engine based on air-fuel ratio control*, Chinese Journal of Aeronautics, Vol. 32, Issue 2, 2019, pp. 489–498. https://doi.org/10.1016/j.cja.2018.10.002

[4] *Aircraft Fuel Supply System with Three Tanks*. For helicopter adaptation, the architecture includes pitch-variable elevation profiles, check valves, centrifugal pumps, and volume-based cutoff controllers tailored to dual-auxiliary-tank configurations.

[5] Yixuan Wang, Yan Shi, Maolin Cai, Weiqing Xu, Qihui Yu,
Efficiency optimized fuel supply strategy of aircraft engine based on air-fuel ratio control,
Chinese Journal of Aeronautics, Vol. 32, Issue 2, 2019, pp. 489–498.
https://doi.org/10.1016/j.cja.2018.10.002

[6] Tomás Gándara, Ernesto Castillo Del Barrio, Marcela Cruchaga, Joan Baiges,
Experimental and numerical modeling of a sloshing problem in a stepped based rectangular tank,
AIP Advances, Vol. 11, No. 3, 2021, Article 035110.
https://doi.org/10.1063/5.0039874